



Faculty of Graduate Studies Chemistry Department

# **Synthesis and Characterization of Graphene Oxide and Magnetic Nanoparticles for Drug Delivery**

By:

**Razan Mohammad Al Hroub**

Supervisor:

**Dr. Sami Makharza**

**This Thesis Submitted in Partial Fulfillment of the Requirements for the  
Degree of Master of Chemistry, College of Graduate Studies & Academic  
Research, Hebron University, Palestine**

2022

## Committee Decision

We, the undersigned, approve the Master's Thesis of Razan Hroub. Thesis Title:

Synthesis and characterization of graphene oxide and magnetic nanoparticles for drug delivery

This thesis was successfully defended on March, 2022 and approved by:

	Committee members	Signature
Supervisor	Dr. Sami Makharza	
Internal Examiner	Mosab Abureesh	
External Examiner	Derar Smadi	

## **Dedication**

I dedicate this thesis to everyone who helped and make it possible, backed me up, whether it was with a phrase or a deed.

To my family, my beloved husband, colleagues, and my supervisor Dr. Sami Makharza, have sent me a special gift.

I'd like to thank the teaching staff at Hebron University chemistry department, as well as the technicians in the chemistry and pharmacy labs, who played a critical role in this project success.

## **Acknowledgment**

At the outset of my thesis, I want to express my heartfelt gratitude to my wonderful parents, and my husband's family for their love and support, special thanks to my husband Eyad AL-Aqabna, without support and encouragement, I would not have been able to complete my studies to my satisfaction, and I do not forget to thank my daughters, Eman and Reman, for their love and support during my research.

I'd like to express my heartfelt gratitude to my supervisor Dr. Sami Makharza, for his support, guidance, assistance, and helpful feedback.

Finally, thank my colleague Majdoleen AL-Atawna for always being there for me during my darkest hours, she always consoled me.

# Table of contents

<b>Dedication</b> .....	<b>i</b>
<b>Acknowledgment</b> .....	<b>ii</b>
<b>Table of contents</b> .....	<b>iii</b>
<b>List of Tables</b> .....	<b>vi</b>
<b>List of Figures</b> .....	<b>vii</b>
<b>List of Abbreviations</b> .....	<b>viii</b>
<b>Abstract</b> .....	<b>ix</b>
<b>Chapter One: Introduction</b> .....	<b>1</b>
1.1 Nanotechnology in Medicine .....	2
1.2 Carbon Nanomaterial .....	3
1.2.1 Fullerene .....	4
1.2.2 Carbon Nanotube ( CNT).....	5
1.2.3 Graphene.....	6
1.3 Magnetism .....	8
1.4 Magnetic nanoparticles .....	10
1.5 Modification of nanoparticles .....	12
1.6 Nanotechnology in cancer therapy .....	13
1.7 Nanosystem for drug delivery.....	15
1.8 Research objectives .....	16
<b>Chapter Two: Literature Review</b> .....	<b>17</b>
2.1 Graphene oxide .....	18
2.2 Magnetite ( Fe <sub>3</sub> O <sub>4</sub> ).....	18
2.3 Graphene oxide / chitosan / magnetite nanocomposites .....	20
<b>Chapter Three: Methodology</b> .....	<b>22</b>

3.1	Materials and Methods .....	23
3.1.1	Chemicals.....	23
3.1.2	Instrumentation.....	23
3.2	Methods .....	23
3.2.1	Preparation of graphite oxide .....	23
3.2.2	Preparation of graphene oxide nanoparticles .....	24
3.2.3	Synthesis of iron oxide particles ( $\text{Fe}_3\text{O}_4$ ) (co-precipitation).....	25
3.2.4	Preparation of graphite oxide- $\text{Fe}_3\text{O}_4$ nanoparticles.....	25
3.2.5	Preparation of graphene oxide- $\text{Fe}_3\text{O}_4$ nanoparticles .....	26
3.2.6	Preparation of graphite oxide with chitosan.....	26
3.2.7	Preparation of graphene oxide with chitosan .....	26
3.2.8	Preparation of graphite oxide-chitosan- $\text{Fe}_3\text{O}_4$ nanoparticles.....	26
3.2.9	Preparation of graphene oxide-chitosan- $\text{Fe}_3\text{O}_4$ nanoparticles .....	27
<b>Chapter Four:Result and Discussion .....</b>		<b>28</b>
4.1	Characterization .....	29
4.1.1	Fourier-transform infrared spectroscopy (FT-IR) .....	29
I.	FT-IR of Graphite, Graphite oxide-450nm, Graphene oxide-200nm .....	29
II.	FT-IR of $\text{Fe}_3\text{O}_4$ .....	30
III.	FT-IR of (GO-450 nm / $\text{Fe}_3\text{O}_4$ ) and (GO-200 nm / $\text{Fe}_3\text{O}_4$ ).....	31
IV.	FT-IR of chitosan .....	32
V.	FT-IR of GO-450 nm /Cs and GO-200 nm /Cs.....	33
VI.	FT-IR of GO-450 nm / Cs / $\text{Fe}_3\text{O}_4$ and GO-200nm / Cs / $\text{Fe}_3\text{O}_4$ .....	35
4.1.2	UV-visible spectrophotometer study .....	36
I.	UV-visible spectroscopy of iron oxide particles .....	36
II.	UV-visible of GO-450 nm and GO-200 nm.....	37
III.	UV-visible of GO-450 nm / $\text{Fe}_3\text{O}_4$ and GO-200 nm / $\text{Fe}_3\text{O}_4$ .....	37

IV. UV-visible of chitosan .....	39
V. UV-visible of GO-450 nm / Cs and GO-200 nm / Cs.....	40
VI. UV-visible of GO-450 nm/Cs/Fe <sub>3</sub> O <sub>4</sub> and GO-200 nm/Cs/Fe <sub>3</sub> O <sub>4</sub> .....	40
4.1.3 Synthesis of Fe <sub>3</sub> O <sub>4</sub> .....	41
4.1.4 Differential scanning calorimetry (DSC).....	42
<b>Chapter Five: Conclusion and Recommendations</b> .....	<b>46</b>
1.1 Conclusion .....	47
1.2 Recommendations .....	47
<b>References</b> .....	<b>48</b>

## List of Tables

<i>Table 1:</i> Examples of nanoparticules used in biological research.....	3
<i>Table 2:</i> Physical properties of magnetite. ....	11
<i>Table 3:</i> Some examples of modified by different materials.....	12

## List of Figure

<b>Figure 1.</b> Allotropes of carbon. ....	4
<b>Figure 2.</b> Single, double and multi walled carbon nanotubes.....	5
<b>Figure 3.</b> Types of single-walled carbon nanotubes. ....	6
<b>Figure 4.</b> Structure of graphene oxide (GO) .....	7
<b>Figure 5.</b> types of materials magnetism .....	9
<b>Figure 6.</b> Structure of chitosan. ....	13
<b>Figure 7.</b> Passive and active targeting of nanoparticles. ....	15
<b>Figure 8.</b> Preparation steps of graphite oxide.....	24
<b>Figure 9.</b> Magnetic nanoparticle during preparation .....	25
<b>Figure 10.</b> FT-IR spectra of (a) graphite, (b) graphite oxide and (c) graphene oxide .....	30
<b>Figure 11.</b> FT-IR spectrum of $\text{Fe}_3\text{O}_4$ . ....	31
<b>Figure 12.</b> FT-IR spectra of (a) GO-450 nm/ $\text{Fe}_3\text{O}_4$ , (b) GO-200 nm/ $\text{Fe}_3\text{O}_4$ . ....	32
<b>Figure 13.</b> FT-IR spectra of chitosan. ....	33
<b>Figure 14.</b> FT-IR spectra of (a)GO-450 nm /Cs and (b) GO-200 nm / Cs .....	34
<b>Figure 15.</b> spectra of (a) GO-450 nm/Cs/ $\text{Fe}_3\text{O}_4$ and (b) GO-200 nm/Cs/ $\text{Fe}_3\text{O}_4$ . ....	35
<b>Figure 16.</b> FT-IR spectra of $\text{Fe}_3\text{O}_4$ , GO-200 nm /Ch and GO-200 nm/Ch/ $\text{Fe}_3\text{O}_4$ .....	35
<b>Figure 17.</b> UV-Vis spectrum of $\text{Fe}_3\text{O}_4$ . ....	36
<b>Figure 18.</b> UV-Vis spectra of GO-450 nm and GO-200 nm. ....	37
<b>Figure 19.</b> UV-Vis spectra of GO-450 nm / $\text{Fe}_3\text{O}_4$ and GO-200 nm / $\text{Fe}_3\text{O}_4$ . ....	38
<b>Figure 20.</b> The separation and redispersion of a solution of GO-200 nm / $\text{Fe}_3\text{O}_4$ in the absence (left) and presence of an external magnetic field (right) .....	38
<b>Figure 21.</b> UV-Vis spectrum of chitosan. ....	39
<b>Figure 22.</b> UV-Vis spectra of GO- 450 nm / Cs and GO-200 nm / Cs . ....	40
<b>Figure 23.</b> UV-Vis spectra of GO-450 nm/Cs/ $\text{Fe}_3\text{O}_4$ and GO-200 nm/Cs/ $\text{Fe}_3\text{O}_4$ .....	41
<b>Figure 24.</b> Magnetic activity of $\text{Fe}_3\text{O}_4$ particles with (a) and without external magnetic field (b).....	42
<b>Figure 25.</b> DSC thermal study of $\text{Fe}_3\text{O}_4$ .....	43
<b>Figure 26.</b> DSC thermal study of GO-200 nm . ....	44
<b>Figure 27.</b> DSC thermal study of GO-200 nm / $\text{Fe}_3\text{O}_4$ . ....	45

## List of Abbreviations

Fe <sub>3</sub> O <sub>4</sub>	Iron(III) oxide
RPM	Rotation per minute
DMF	N,N-Dimethylformamide (C <sub>3</sub> H <sub>7</sub> NO)
Ø	pour size of filter paper
FT-IR	Fourier-transform infrared spectroscopy
MNPs	Magnetic nanoparticles
UV-Vis	Ultraviolet – visible absorption spectroscopy
GO- 450 nm	Graphite oxide-450 nm
GO- 200 nm	Graphene oxide-200 nm
DSC	Differential Scanning Calorimetry
Cs	Chitosan
CNTs	Carbon nanotubes
SWCNTs	Single-walled carbon nanotubes
DWCNTs	Double-walled carbon nanotubes
MWCNTs	Multi-walled carbon nanotubes
D.W	Distilled water

## Abstract

In this thesis we have prepared and characterize two sizes of GO (450 and 200 nm). As well as, magnetic based iron oxide particles have been prepared and loaded on GO and functionalized GO based on chitosan molecules.

The oxidation-reduction process was used to make graphite oxide (Hummers method), and the end product was designated graphite oxide as prepare (GO- 450 nm), Under controlled conditions, a tip sonicator was used to decrease the particle size to 200 nm (time and power of sonication). A simple chemical reaction (Co-precipitation) between  $Fe^{+3}$  and  $Fe^{+2}$  produces magnetic iron oxide particles called  $Fe_3O_4$ .

FT-IR spectroscopy reveals that two sizes of GO particles (GO-450 nm and GO-200 nm) have different types of oxygen groups on their surfaces, and the FT-IR spectrum of prepared  $Fe_3O_4$  are shown a strong peak at around  $588\text{ cm}^{-1}$  proving that the formation of magnetic particles is performed. FT-IR spectra of (GO-200 nm/Cs/ $Fe_3O_4$ ) exhibit sharp peak than (GO-450 nm/Cs/ $Fe_3O_4$ ). DSC of  $Fe_3O_4$ , GO-200 nm and GO-200 nm/ $Fe_3O_4$  for identification the structure. The UV- visible spectroscopy for two system{ (GO-450 nm/Cs/ $Fe_3O_4$ ), (GO-200 nm/Cs/ $Fe_3O_4$ )} revealed the bandwidth increase with decreasing the size of nanoparticles.

# **Chapter One:**

# **Introduction**

## 1.1 Nanotechnology in Medicine

Nanotechnology is a large and multidisciplinary field of study and development that has grown significantly in recent decades. Purposefully influencing matter at the nanoscale is a new idea, first proposed by Richard Feynman in a presentation to the American Physical Society in 1959 titled "There is plenty of room at the bottom: an invitation to enter a new field of physics." [1]. In 1974, the term 'nanotechnology' was first given by a Japanese scientist, Prof Norio Taniguchi (University of Tokyo). Nanotechnology is the study and control of materials with dimensions ranging from 1 to 100 nanometers, allowing for unique size-dependent characteristics [2]. The word "nano" comes from the Greek word "dwarf". Hence, a nanometer (nm) is one billionth of a meter.

Nanomaterials are believed to be significantly more reactive than bulk materials because they have a large surface area and a high fraction of atoms at the surface. As a result, the physical and chemical characteristics of these nanostructure materials differ significantly from those of a single atom (molecule) and bulk material of similar chemical structure. These nanostructures are incredibly tiny once produced, and they produce some unique and intriguing electrical, optical, structural, and electromagnetic characteristics in nanomaterials. Nanomaterials have attracted a lot of interest and are being used for a variety of applications in textiles, drug delivery, energy storage systems, cosmetics, microelectronics, and healthcare due to their unique and advantageous physical, chemical, and mechanical characteristics [3].

In nanomedicine, which is the use of nanotechnology in medicine, nano-scaled materials and nano electronic biosensors are used to diagnose, monitor, follow-up, and prevent illnesses. Many diseases today, ranging from diabetes to cancer to Parkinson's and Alzheimer's, pose a serious danger to human life, and precise diagnosis is critical for proper treatment. Nanosensors and nanoparticles made using nanotechnology are critical for accurate diagnosis and rapid treatment [4].

Ultrasensitive and selective multiplexed diagnostics, drug delivery, targeted treatment of cancer and other illnesses, body imaging, tissue/organ regeneration, and gene therapy are the most potential future nanoscience-based uses in medicine. All of these applications combine technical advancements with better biological system manipulation methods [5]. Table 1 shows some nanoparticles used in biological research.

**Table 1:** Examples of nanoparticles used in biological research

<b>Nanoparticle</b>	<b>Application</b>	<b>Reference</b>
Magnetic nanoparticles	Specific targeting of cancer cells, tissue imaging	[6]
Silicon-based nanowires	Real-time detection and titration of antibodies, virus detection, chip-based biosensors	[7],[8]
Carbon nanotubes	Electronic biosensors	[9]
polymer–drug nanoparticles	Colorectal cancer, lung metastasis treatment	[10]
graphene oxide nanoparticle functionalized with polyethylene glycol and folic acid	anticancer drug delivery	[11]
silver nanoparticles	treatment of lung cancer	[12]
Fluorescent nanodiamond	repair of lung stem cells	[13]

## 1.2 Carbon Nanomaterial

Carbon is an element with atomic number 6. The periodic table of the elements places it in group IV. The ability of some chemical elements to form a variety of molecular shapes from the same kind of atoms is known as "allotropy". Graphite, diamond are carbon allotropes[14].

The carbon atoms in graphite are  $sp^2$  hybridized, meaning that each carbon has three covalent bonds ( $\sigma$  bonds) with three other carbons in the same plane. The fourth valence electron that is not involved in the  $sp^2$  hybridization is delocalized through  $\pi$ - $\pi$  interaction, resulting in in-plane metallic bonding. As a result, the bonding inside the layer is a combination of covalent and metallic bonding. The neighboring layers, on the other hand, are weakly bonded by van der Waals forces, but the carbon atoms in diamond have been  $sp^3$  hybridized, which means that each carbon atom has four covalent bonds ( $\sigma$  bonds) that are directed tetrahedrally to four other carbon atoms. There are no free electrons since all of the valence electrons are involved in covalent bonds. Diamond, as a result, is an electrical insulator[15].

Meanwhile, various new allotropic forms have been described, including carbon nanomaterials, the most popular method for classifying carbon-based nanomaterials is to look at their geometrical structure. Carbon nanostructures can be tube-shaped, horn-shaped, spherical, or ellipsoidal in form. Carbon nanotubes are tube-shaped particles; nanohorns are horn-shaped particles; fullerenes are spheres or ellipsoids; and graphene is a single layer (monolayer) of carbon atoms (figure 1) [16].

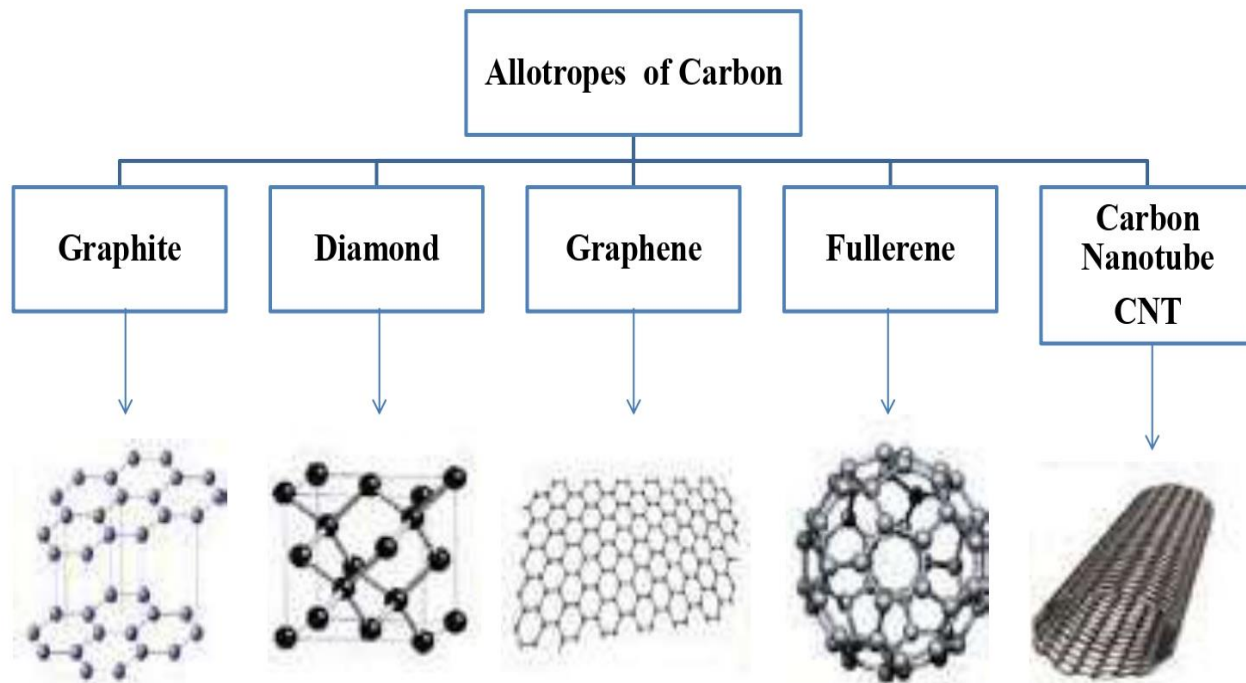


*Figure 1.* Allotropes of carbon.

### 1.2.1 Fullerene

In 1985 the fullerene was discovered by H.W. Kroto, R.F. Curl and R.E. Smalley [17], Fullerene is the  $C_{60}$  molecule, which is made up entirely of carbon atoms and contains no other elements. The molecule has the shape of a ball, with diameter about 0.7 nm [18]. Each carbon atom is connected to three other carbon atoms by three bonds, and it is frequently found near the vertices of pentagons and hexagons on the sphere's surface. The word fullerene was coined in honor of Buckminster Fuller, an American architect who created a huge geodesic dome that

mirrored the molecular structure of  $C_{60}$ . Bucky balls are the name for these balls, other possible fullerene structures are  $C_{20}$ ,  $C_{24}$ ,  $C_{28}$ ,  $C_{32}$ ,  $C_{36}$ , and  $C_{60}$ . Fullerenes are employed as catalysts, lubricants, and carriers for delivering drugs into the body [15].

### 1.2.2 Carbon Nanotube (CNT)

CNTs are a type of carbon allotrope with unique characteristics that make them ideal for technological applications, S. Iijima, a Japanese researcher, discovered CNTs in 1991 [19]. Carbon nanotubes are cylindrical structures made up of rolled graphene sheets with a diameter of several nanometers. The length, diameter, chirality (symmetry of the rolled graphite sheet), and number of layers of carbon nanotubes can all vary. CNTs are divided into three types based on their structure: single-walled carbon nanotubes (SWCNTs), multi-walled carbon nanotubes (MWCNTs) figure 2 [20], and double-walled carbon nanotubes (DWCNTs) [21].

SWCNTs are made up of a single cylindrical carbon layer with a few micrometers in length and diameter ranging from 0.4 to 2 nanometers, depending on the temperature at which they were made. It was discovered that the bigger the diameter of CNTs is, the higher the growing temperature. MWCNTs are made up of several coaxial cylinders. MWCNTs have an outside diameter of 2 to 100 nanometers, an inside diameter of 1-3 nanometers, and a length of one to several micrometers [22].

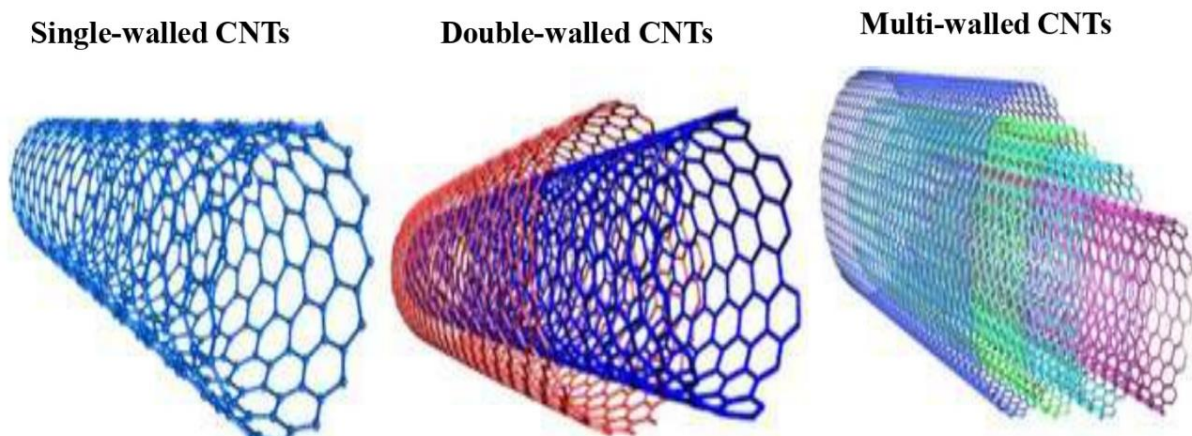


*Figure 2.* Single, double and multi walled carbon nanotubes.

When compared to other fibrous materials, CNTs have a unique mix of rigidity, strength, and elasticity due to their structure. In comparison to other conductive materials, CNTs have a high thermal and electrical conductivity [23]. The chirality or hexagon orientation of SWCNTs with respect to the tube axis determines their electrical characteristics. SWCNTs are divided into three sub-classes based on their electrical conductivity: (i) armchair (electrical conductivity > copper), (ii) zigzag (semi-conductive characteristics), and (iii) chiral (semi-conductive characteristics) as exhibited in figure 3 [16].

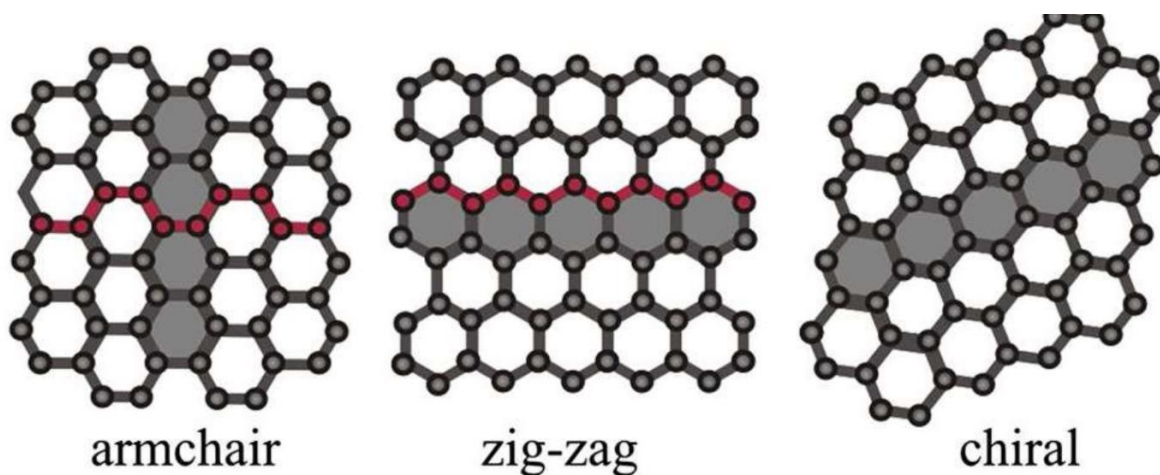


*Figure 3.* Types of single-walled carbon nanotubes.

CNTs' functionalization allows them to be used in a variety of applications. Because of their construction, the tubes contain an inner and outer core, both of which may be changed by different functional groups. As a result, CNTs may be tailored to specific applications. The uses of carbon nanotubes in biomedicine are being studied in four primary areas: drug delivery, biomedical imaging, biosensors, and tissue engineering scaffolds [24].

### 1.2.3 Graphene

Graphene is a two-dimensional allotropic carbon material made up of single carbon atom layers as shown in figure 1. Carbon atoms in graphene show  $sp^2$ -hybridization in a two-

dimensional hexagonal crystal lattice linked by  $\sigma$  and  $\pi$  bonds. Other carbon allotropes, such as graphite, carbon nanotubes, and fullerenes, contain graphene as a structural constituent.

Theoretical graphene research began long before actual material samples were obtained. P. R. Wallace, a Canadian theoretical physicist, was the first to investigate the theory of graphene in 1947, while A. Geim (a Dutch-British physicist) and K. Novoselov (a Russian-British physicist) described the first graphene samples 57 years later (in 2004), and were awarded the Nobel Prize in 2010 [25].

High conductivity, huge surface area, and mechanical and thermal durability are only a few of the amazing features of graphene. These characteristics make graphene a useful material in a variety of applications, including fuel cell catalysis, supercapacitors, photocatalysis, heterogeneous catalysis, water purification, drug delivery, and biosensing [26]. Graphene is a highly hydrophobic material that does not dissolve in hydrophilic solvents and collects into huge aggregates. Graphene oxide (GO) (figure 4 [27]) is a frequently applied option to solve this problem.

Chemical exfoliation of graphite powder with a strong oxidizing reagent yields extremely colloidally stable exfoliated hydrophilic GO sheets. Carbons with  $sp^2$  ( $C=C$ ,  $C=O$ ) and  $sp^3$  ( $C-C$ ,  $C-OH$ ,  $C-O-C$ ) hybridization, as well as oxygen functionality such as hydroxyl, epoxy, carbonyl, and carboxyl groups, are found in GO [28].

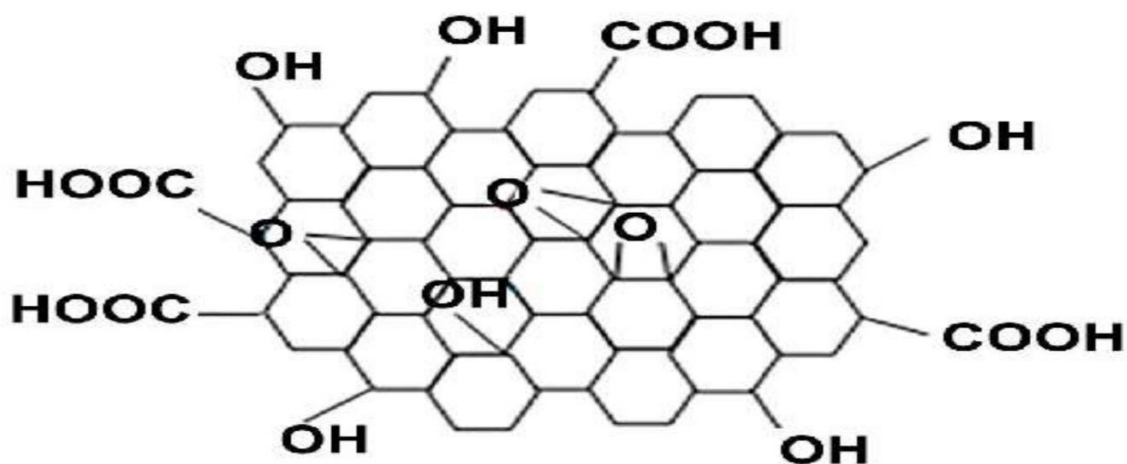


*Figure 4.* Structure of graphene oxide (GO)

## 1.3 Magnetism

The alignment of the electron spin causes magnetism or magnetic effects in a substance. The spin of electric-charged particles (electrons, holes, protons, positive and negative ions) with both mass and electric charges can result in the formation of a magnetic dipole, or magneton. Thus, materials' magnetism may be divided into five fundamental kinds, namely **paramagnetism**, **diamagnetism**, **ferromagnetism**, **ferrimagnetisms**, and **antiferromagnetism** as shown in figure 5 [29], based on their reactions to an external magnetic field and the orientation of magnetic moments in materials [30].

Very weak; exists only in presence of an external field, non-permanent, because the applied external field acts on atoms of a material, slightly unbalancing their orbiting electrons, and creates small magnetic dipoles within atoms which that oppose the applied field. This action produces a negative magnetic effect known as **diamagnetism**, such as Cu, Ag, Si, Ag and alumina are diamagnetic at room temperature [31].

Slightly stronger; dipoles line up with the field when an external field is introduced, resulting in positive magnetization. Para-magnetic materials are those that have a modest positive magnetic susceptibility in the presence of a magnetic field. The orientations of atomic magnetic moments are random in the absence of an external field, resulting in no net magnetization; nevertheless, when an external field is introduced, dipoles line up with the field, resulting in positive magnetization. Furthermore, if the magnetic field is removed, the effect is gone. Many materials, such as aluminum, calcium, titanium, and copper alloys, cause **paramagnetism** [32].

Because magnetization occurs only in the presence of an external field, both dia- and para-magnetic materials are classified as non-magnetic. However, even in the absence of an external field, certain materials have permanent magnetic moments. This is due to unfilled energy levels forming permanent unpaired dipoles. Due to the exchange interaction or mutual reinforcement of the dipoles, these dipoles can easily line up with the imposed magnetic field. These are **ferromagnetic** chrematistics. Ferromagnetism materials (examples: Fe, Co, Ni, Gd) Ferro magnets are extremely powerful; when an external field is applied, the dipoles line up permanently. There are two sub-classes in this class: Anti-ferromagnetism, and Ferrimagnetisms.



## 1.4 Magnetic nanoparticles

Magnetic nanoparticles abound in nature and can be discovered in a variety of biological structures, where used in information storage and retrieval systems, new permanent magnets, magnetic cooling systems, magnetic sensors, biomedicine, and catalysis, as well as contrast agents for magnetic resonance imaging and cancer therapy agents [33].

Iron oxide nanoparticles are the most often used magnetic nanoparticles, while may be found in nature in a variety of structures and phases, including oxides, oxyhydroxides, and hydroxides. At ambient pressure, six phases of iron oxides can occur, including magnetite  $\text{Fe}_3\text{O}_4$ , wustite  $\text{FeO}$ , and  $\text{Fe}_2\text{O}_3$  ( $\alpha$ - $\text{Fe}_2\text{O}_3$ ,  $\gamma$ - $\text{Fe}_2\text{O}_3$ ,  $\beta$ - $\text{Fe}_2\text{O}_3$ , and  $\epsilon$ - $\text{Fe}_2\text{O}_3$ ).  $\text{Fe}_3\text{O}_4$  (magnetite),  $\alpha$ - $\text{Fe}_2\text{O}_3$  (hematite),  $\gamma$ - $\text{Fe}_2\text{O}_3$  (maghemite), and  $\text{FeO}$  (wustite) are the most frequent ferrous and ferric oxides that are researched because of their unique properties at the nanoscale. Furthermore, these iron oxides have strong magnetic properties in nature, surface enhancement and functionalization of these magnetic oxides at nanometric dimensions has a lot of applications, including biomedical, catalysts, batteries, magnetic resonance imaging agents (MRI), and biosensing [34].

Black iron oxide, magnetic iron ore, loadstone, ferrous ferrite, and Hercules stone are all names for magnetite ( $\text{Fe}_3\text{O}_4$ ), and it has the highest magnetic properties of any transition metal oxide. Close-packed planes of oxygen anions with iron cations in octahedral or tetrahedral interstitial sites characterize the magnetite crystal structure [35]. The oxygen ions in magnetite are arranged in a cubic close-packed configuration. With  $\text{Fe(III)}$  ions distributed randomly between octahedral and tetrahedral sites, and  $\text{Fe(II)}$  ions in octahedral sites, magnetite exhibits an inverse spinel structure [36].

The active electrons in the 3d orbitals give magnetite its unique electronic and ferromagnetic characteristics (unpaired electron spins), wherefore; in room temperature, magnetite is a ferromagnetic substance, and It is a naturally occurring mineral that has the highest magnetic of any transition metal oxide. The following table summarizes some of the physical properties of magnetite [35].

**Table 2:** Physical properties of magnetite.

Property	Magnetite
Molecular formula	Fe <sub>3</sub> O <sub>4</sub>
Density (g/cm <sup>3</sup> )	5.18
Melting point (°C)	1583 - 1597
Hardness	5.5
Type of magnetism	Ferromagnetic
Standard free energy of formation $\Delta G^{\circ}_f$ (kJ/mol)	-1012.6

Various techniques, including as co-precipitation, hydrothermal, thermal decomposition, and the sol-gel technique, have been used to synthesize magnetite (Fe<sub>3</sub>O<sub>4</sub>) nanoparticles [37]. Magnetite nanoparticles have been studied for a variety of uses, including rapid magnetic separation, improved sensitivity in magnetic resonance imaging (MRI) contrast agents, high drug loading capacity nanocarriers, and magnetically responsive photonic crystals. Furthermore, nanotechnology has the potential to build biomedical nanoplatforms for cancer therapy. Magnetic nanoparticles, which combine some of the most appealing properties of magnetic manipulation [38].

Magnetite nanoparticles with cell membrane coatings have recently been developed for tumor targeting and drug delivery. Macrophage membrane-coated magnetic nanoparticles, for example, have been shown to be effective nanocarriers for tumor targeting and treatment [39]. The functioning transmembrane receptors in that study were able to identify cancer cells through cell-cell adhesion between macrophage and cancer cell surfaces, allowing for efficient cell targeting. Similar principles have also been proven for membrane-coated magnetic nanoparticles made from myeloid-derived suppressor cells, which worked well in immune evasion and active tumor targeting. In another hand, the optical applications of magnetic nanoparticles, The optical response of magnetic nanoclusters of various clusters and grain sizes were tested. It was revealed that there was a critical nanocluster size (40 nm) below which no changes in light diffraction with applied magnetic fields could be seen. Furthermore, bigger nanoclusters (>160 nm) diffracted red light in low magnetic fields, but smaller nanoclusters (100 nm) diffracted blue light in higher magnetic fields [40].

## 1.5 Modification of nanoparticles

The physical-chemical modification of nanoparticles is an essential step for (a) passivating a highly reactive nanoparticle, (b) stabilizing a highly aggregative nanoparticle in a medium (such as a solvent or a polymer melt) in which the nanoparticles are to be dispersed, (c) functionalizing the nanoparticle for applications such as molecular recognition, or (d) promoting nanoparticle assembly. Grafting thiolated surfactants or polymers, adsorption of charged surfactants, charged ligands, or polymer brushes, attachment of biological molecules such as DNA, peptides, proteins, antigens, or coating a continuous polymer film on nanoparticles are some of the most commonly used surface modification methods [41]. In table 3 some example of nanoparticles modification by different material.

*Table 3:* Some examples of modified by different materials

<b>Modified nanoparticles</b>	<b>Surface modification by</b>	<b>Reason of modification</b>	<b>Reference</b>
<b>Magnetite nanoparticles</b>	Poly(ethylene glycol)(PEG) and folic acid	To improve their intracellular uptake and ability to target specific cells.	[42]
<b>Graphene oxide (GO)</b>	Magnetite nanoparticles (Fe <sub>3</sub> O <sub>4</sub> )	the convenient separation of the GO from the sample, given from the Fe <sub>3</sub> O <sub>4</sub> by using external magnetic field	[43]
<b>zinc oxide nanoparticles</b>	Polymethacrylic acid (PMAA)	PMAA-modified zinc oxide presented a stable colloidal dispersion for a long time.	[44]

The polymers that are often used to modify nanoparticles, synthetic polymers can be either hydrophobic or hydrophilic, but natural polymers are more likely to be hydrophilic. Chitosan as shown in figure 6 [45] is the second most abundant natural biopolymer after cellulose, and is derived from crustacean shells. Chitosan is a cationic polysaccharide that is made by chemical deacetylation of chitin [46]. The degree of deacetylation and molecular weight of chitosan depending on source of chitin, affect the physicochemical characteristics (solubility, toxicity, and hydrophobicity) of the substance.

## Chitosan

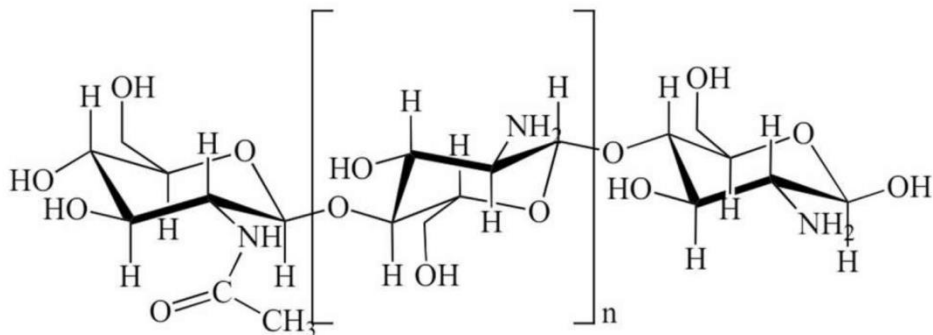


*Figure 6.* Structure of chitosan.

Chitosan is insoluble in water, organic solvents, and aqueous bases, but it dissolves in acids like acetic, nitric, hydrochloric, perchloric, and phosphoric after stirring [47].

Chitosan's unique properties (mucoadhesion, controlled drug release, permeation enhancement, biocompatibility and biodegradability, and antibacterial and antifungal activity) make it useful in a variety of industries, including pharmaceuticals, agriculture, food, and bioengineering [48].

### 1.6 Nanotechnology in cancer therapy

Cancer is produced by a combination of genetic and non-genetic variations produced by environmental factors, which result in the improper activation or inactivation of specific genes, resulting in neoplastic transformations or abnormal cell proliferation. There is a scarcity of knowledge about critical cellular processes that occur early in the genesis of cancer, as well as the environmental factors and internal signals that cause these changes. The type and location of the cancer, as well as the patient's financial ability to pay for therapy, all determine the cancer treatment that a patient receives. Surgery is the most common and successful type of first cancer treatment for most solid tumors, especially if the cancer is still in its early stages. Because the objective is curative treatment, this is frequently coupled with radiation therapy to the tumor bed and systemic therapy. Radiation, chemotherapy, hormone ablation therapy, and hormone ablation therapy are common therapies as cancers develop. In suitable cases, targeted treatment is becoming more widely available [49].

The use of nanoparticles for the detection and treatment of cancers in the human body is an important use of nanotechnology in medicine. Although this is still a new method, it will be a potential cancer therapy option.

The location of cancerous tissues may be detected using iron oxide nanoparticles with magnetic characteristics, which can be used to detect cancer. First, the body is injected with specific antibodies marked with iron oxide nanoparticles that have been created against the tumor being sought. Marked antibodies bind to antigens on the tumor surface if the desired tumor cannot be detected in the body. The magnetic signals generated by the iron oxide particles contained in the antibodies collected in the cancerous tissue can be used to detect tumors with a magnetic resonance imaging (MRI) device. It is possible to identify even the tiny tumor tissue in the body [50].

Nanoparticles must be stable at a pH of 7 in water or a physiological environment for uses in biology, therapy, and medical diagnostics. Furthermore, the nanoparticles must be non-immunogenic, have a large effective surface area, have low sedimentation, and have improved tissular diffusion to prevent vessel embolism, allow the binding and delivery of targeted drugs or biomolecules to a specific area via entrapment, adsorption, or covalent interaction, and to remain in the circulation or pass through the capillary system after an injection [35].

Tumor targeting is one of the possible basic advantages of nanotechnology for cancer treatment. Nanotechnology's aim in cancer therapy is to be able to distinguish malignant cells from nonmalignant cells and to selectively eliminate malignant cells. Passive and active targeting are two main mechanisms involved in the differentiation of malignant and nonmalignant cells. The enhanced permeability and retention (EPR) effect is used in passive targeting to increase the concentration of nanoparticles (NPs) in the tumor, to localize nanoparticles (NPs) to malignant cells [51], active targeting may entail selective molecular recognition of antigens (figure.7 [52]), most often proteins, expressed on the surfaces of cancer cells, or alternatively, exploiting biochemical characteristics associated with malignancy such as matrix metalloproteinase release [53]. Both passive and active targeting techniques can be used separately or in combination. Surface modifications of NPs help both techniques by reducing absorption by the macrophage phagocytic system (MPS) and therefore maximizing duration in circulation [54].

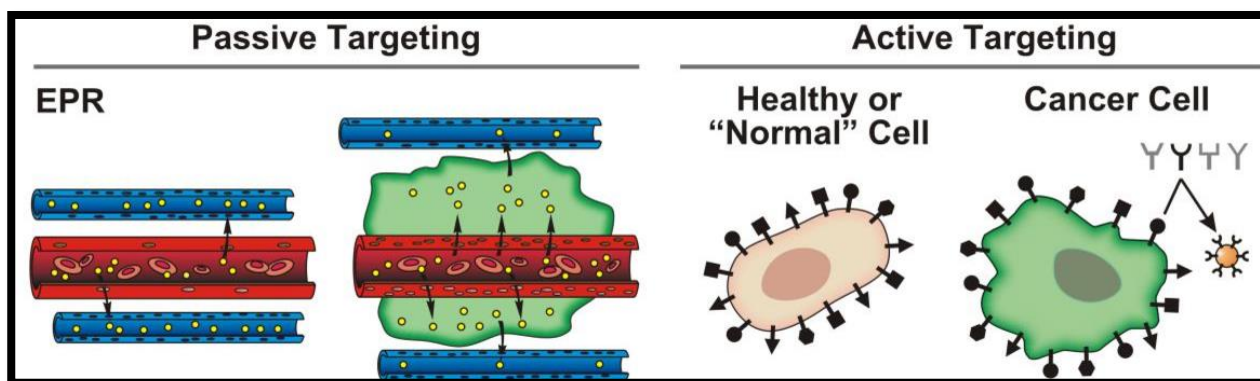


*Figure 7.* Passive and active targeting of nanoparticles.

## 1.7 Nanosystem for drug delivery

One of the most important applications of nanotechnology in medicine is drug delivery, which is the subject of several research. It is possible to identify diseased cells, such as cancer cells, by injecting medicines that are coated with nanoparticles. Nanoparticles transport the medicines they contain to diseased cells, allowing the body to eliminate them without hurting healthy ones [50].

A drug molecule's therapeutic potential is determined by its availability at the target location in the needed amount and for the required duration. To avoid potential side effects, it's also critical to limit the drug's exposure to non-target tissues. More than 70% of newly discovered small molecules are hydrophobic and have low water solubility, which limits their ability to be carried by blood and other bodily fluids [55]. Furthermore, certain medicines have a short half-life and residence duration due to fast clearance. It's a problem to get a medication to the correct spot, at the right concentration, and for the right amount of time. Some of these problems can be solved by incorporating the drug into an appropriate delivery system.

Drug delivery methods improve the drug's pharmacokinetic characteristics (distribution, absorption, distribution, and elimination) to enhance effectiveness and safety. The use of carriers with a diameter of less than 100nm for medication delivery has received a lot of attention in the last two decades. Because the smallest blood capillaries are 10–20  $\mu\text{m}$  in diameter, this particle size range allows for systemic delivery. In addition, carriers in this size range might be used to deliver various therapeutic payloads to specific organs and tissues [56]. Lipid nanoparticles,

micelles, polymeric conjugates, solid-lipid nanoparticles, and inorganic nanoparticles have all been created as nano-delivery systems with various topologies. Pre-clinical activity in illnesses including AIDS, cancer, malaria, diabetes, and tuberculosis has been hopeful, and some of these systems have already been allowed for human use [57].

Some example for using magnetic nanoparticles in drug delivery system. Iron oxide nanoclusters have been employed in biological applications such as magnetically triggered drug release and high-sensitivity MRI contrast agents. Iron oxide nanoparticles (>10 nm) and drugs were colocalized in nanocarriers for magnetically induced drug release, or porous iron oxide nanoclusters were produced to maximize drug loading by surface adsorption. Local heat was created by iron oxide nanoparticles under alternating magnetic fields (AMFs), which raised local temperatures and induced drug release [58].

## 1.8 Research objectives

The main objectives of this study are :

- I.* Synthesis and characterization of graphene oxide nanoparticles with two size graphene oxide (GO-450 nm ), and graphene oxide (GO-200 nm).
- II.* Synthesis of magnetic iron(III) oxide particles ( $\text{Fe}_3\text{O}_4$ ) with excellent properties using a simple and environmentally safe in-situ chemical synthesis method at room temperature (co-precipitation).
- III.* Synthesis and characterization of graphene oxide – chitosan –  $\text{Fe}_3\text{O}_4$  as delivery system.

# **Chapter Two: Literature Review**

## 2.1 Graphene oxide

The graphene oxide (GO) synthesis process is an important step to note since the yield GO determines and is highly reliant on the optimal characteristics shown by GO at the nanoscale for all possible applications. Many prepared GO sheets routes have been developed and reported up to date. In general, graphene production techniques include exfoliation of graphite oxide by Brodie in 1859 [28], Staudenmaier method [59], Hummer's methods [60], and water electrolytic oxidation of graphite in 2018 [61].

Both Brodie and Staudenmaier used potassium chlorate ( $\text{KClO}_3$ ) and fuming nitric acid for oxidation, but in Staudenmaier method used sulfuric acid to increase the acidity of the mixture, finally product in both these method was at risk of exploding. Potassium permanganate and sulfuric acid are used in the Hummer's technique.

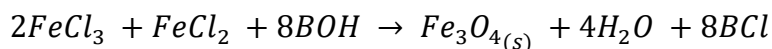
Water electrolytic oxidation of graphite produces clean GO sheets in a scalable, safe, ultrafast, and environmentally friendly way. It has been shown that pre-intercalation of graphite at high voltage effectively inhibits the anodic electrocatalytic oxygen evolution process of water, allowing for rapid oxidation of graphene lattice in a few seconds, which is over 100 times quicker than current techniques. The GO produced has a chemical composition, structure, and characteristics that are similar to those generated by the traditional Hummers technique [61].

## 2.2 Magnetite ( $\text{Fe}_3\text{O}_4$ )

The choice of a suitable magnetite preparation technique has a significant impact on and defines the interesting characteristics of synthesized iron oxides in their prospective applications. Up to now, a significant deal of work has gone into developing ways for making magnetic nanoparticles that are extremely stable, nanosized and structure regulated, have a limited size distribution, excellent crystallinity, and have a strong magnetic nature. Some common synthetic processes include co-precipitation, hydrothermal, solvothermal, sol-gel, microemulsion, sonochemical, microwave-assisted, and electrochemical techniques [62].

The most practical and easy approach for producing black magnetic iron oxide from a combination of aqueous salt solutions is co-precipitation. This technique of precipitation includes combining ferrous ( $\text{Fe}^{2+}$ ) and ferric ( $\text{Fe}^{3+}$ ) ions in a 1:2 molar ratio with alkaline solution at room

temperature or high temperature. The whole chemical process is described here, with BOH denoting various bases, such as Na<sup>+</sup>, K<sup>+</sup>, or (C<sub>2</sub>H<sub>5</sub>)<sub>4</sub>N<sup>+</sup> [63].



Furthermore, critical factors such as the media's ionic strength, Fe<sup>3+</sup>/Fe<sup>2+</sup> ratio, pH value, reaction temperature, mixing rate, and the kinds of salt employed all have a significant impact on the production of nanosized iron oxide particles. However, the generated iron oxide particles from this pathway have a wide particle size distribution, are unstable, and easily oxidize to maghemite in the air or agglomerate, so adding surfactants or stabilizers and bubbling nitrogen gas are recommended to generate good crystallinity and stabilized magnetite nanoparticles [64].

The water in oil (W/O) microemulsion is a thermodynamically stable single phase system dispersion made up of two immiscible phases in the presence of a surfactant, which is widely employed in the production of uniformly sized superparamagnetic nanoparticles. The addition of a surfactant to a mixed system lowers the interfacial tension between water and oil, allowing a clear solution to develop. Despite the inclusion of surfactants, a stabilization treatment procedure employing stabilizers during manufacturing is required to prevent the nanoparticles from aggregating. However, one disadvantage of this synthesis route is that it requires a huge amount of solvent but produces a little amount of yield [65].

The hydrothermal, or solvothermal, method of producing extremely crystalline, ultrafine, and pure magnetite particles is both efficient and environmentally safe. This reaction system must be carried out in an aqueous medium in reactors or autoclaves with pressures and temperatures more than 200 psi and 200 °C. The hydrothermal technique, on the other hand, has slow reaction kinetics at any temperature. As a result, a microwave-hydrothermal technique is combined to improve crystallization kinetics for the manufacture of higher crystallinity and purity magnetic nanoparticles [66].

The sonochemical technique, which is based on the sonic cavitation phenomena, is commonly used to manufacture extremely monodispersive nanosized materials with appealing characteristics in a short response time. The ultrasonication of a mixture comprising Fe(II) or Fe(III) complexes or iron salts in an inert environment results in a narrow particle size distribution of the end product in the sonochemical synthesis of magnetite [67].

## 2.3 Graphene oxide / chitosan / magnetite nanocomposites

Magnetic graphene films have been described in recent studies for a variety of uses. Materials combining graphene oxide and magnetite nanoparticles ( $\text{Fe}_3\text{O}_4$ ) have shown intriguing improved characteristics. Surface modification of  $\text{Fe}_3\text{O}_4$  is required to improve the chemical stability of it. In addition to its nontoxicity, biocompatibility, biodegradability, bioactivity, and solubility in aqueous media [68], chitosan is a natural polymer biomaterial. Furthermore, due of the amino and hydroxyl groups in its structure, chitosan is a good candidate for chemical modification. There have also been several studies on chitosan-coated magnetite nanocomposites [69]. Graphene oxide or graphene modified with chitosan has also been effectively produced recently [70].

Nengsheng Ye and his team successful in synthesis a magnetite/graphene oxide/chitosan ( $\text{Fe}_3\text{O}_4/\text{GO}/\text{Cs}$ ) composite, a simple and innovative approach was devised in 2014. In this study, a simple and novel method of mixing  $\text{Fe}_3\text{O}_4$ , graphene oxide, and chitosan was discovered.  $\text{Fe}_3\text{O}_4$  nanoparticles was produced via chemical co-precipitation of  $\text{FeCl}_3 \cdot 6\text{H}_2\text{O}$  and  $\text{FeCl}_2 \cdot 4\text{H}_2\text{O}$ , followed by the addition of  $\text{Fe}_3\text{O}_4$  to the exfoliated GO solution. To make the  $\text{Fe}_3\text{O}_4/\text{GO}/\text{Cs}$  nanocomposite, chitosan was added to the  $\text{Fe}_3\text{O}_4/\text{GO}$  dispersion solution. The magnetic composite  $\text{Fe}_3\text{O}_4/\text{GO}/\text{Cs}$  was used as an absorbent for protein enrichment, and protein cytochrome c was chosen as a model target, due to the large specific surface area and  $\pi-\pi$  electrostatic stacking property of graphene oxide, hydrophilicity and biocompatibility of chitosan, good biocompatibility and strong superparamagnetic properties of  $\text{Fe}_3\text{O}_4$  [71]. In another study, with the same nanocomposite ( $\text{Fe}_3\text{O}_4/\text{graphene oxide}/\text{chitosan}$ ), Luyen T. Tran and research team were able to manufacture ( $\text{Fe}_3\text{O}_4/\text{graphene oxide}/\text{chitosan}$ ) nanocomposite by using the co-precipitation method to remove nickel ion  $\text{Ni}(\text{II})$  from aqueous solution via the adsorption procedure [72].

In 2017, Hoang V Tran and his team successfully the removal of methylene blue (MB) by using chitosan/ $\text{Fe}_3\text{O}_4$ /graphene oxide ( $\text{Cs}/\text{Fe}_3\text{O}_4/\text{GO}$ ) nanocomposite. To achieve this, graphene oxide (GO) was first produced using Hummer's technique from pencil graphite, and then  $\text{Cs}/\text{Fe}_3\text{O}_4/\text{GO}$  was synthesized using a chemical co-precipitation approach from a mixed solution of GO,  $\text{Fe}^{3+}$ ,  $\text{Fe}^{2+}$ , and chitosan [73].

In 2018, Bei Zhang and his team successful in synthesis a chitosan/magnetite-graphene oxide composites were made using a simple chemical method, in this research used this composites to removal hexavalent chromium Cr(VI) and trivalent chromium Cr(III) from aqueous solution [74].

In 2021, Shabnam Kazemi from Islamic Azad University, Iran and his team successful in synthesis a chitosan-magnetite-reduced graphene oxide (Cs/Fe<sub>3</sub>O<sub>4</sub>/rGO) nanocomposites. In this study, chitosan-magnetite-reduced graphene oxide (Cs/Fe<sub>3</sub>O<sub>4</sub>/rGO) nanocomposites were used to deliver curcumin (Cur) as an anticancer medication to MCF-7 breast cancer cells using a simple water-in-oil (W/O) emulsification process. During future research, the findings of this work are predicted to be useful in the development of targeted drug delivery as well as the development of Cs/Fe<sub>3</sub>O<sub>4</sub>/rGO-based drug carriers against different cancer cells [75].

# **Chapter Three:**

# **Methodology**

## 3.1 Materials and Methods

In this chapter, the experimental details for this study are presented, including the chemicals and materials, and instrumentations used. The preparation method for GO nanoparticles with different two sizes ( GO-450 nm, GO-200 nm) [76], preparation of magnetic nanoparticles ( $\text{Fe}_3\text{O}_4$ ), synthesis of GO/ $\text{Fe}_3\text{O}_4$ , synthesis of GO/chitosan, and composition of GO/chitosan / $\text{Fe}_3\text{O}_4$  (with different two sizes of GO).

### 3.1.1 Chemicals

Graphite powder,  $<20\mu\text{m}$ , potassium permanganate (99%), were purchased from Sigma Aldrich. Sulfuric acid (95%), hydrochloric acid (32%), sodium chloride (99.9%), hydrogen peroxide (30%), sodium hydroxide (99%), Iron(III) chloride hexahydrate, Iron (II) sulfate heptahydrate, DMF (N,N-Dimethylformamide) (99.8%), chloroform, and chitosan (Technical grade). Were used without further purification.

### 3.1.2 Instrumentation

Graphene oxide was characterized using Perkin-Elmer, Spectrum Two, FT-IR spectrometer that has a range of ( $4000\text{--}400\text{ cm}^{-1}$ ). Ultrasonic processors Sonics, Materials VC-750-220, Fisher Scientific. The DSC images were obtained using differential scanning calorimetry, the thermal history of materials was performed in a PerkinElmer Jade DSC at a heating rate of  $10^\circ\text{C}/\text{min}$  from  $35^\circ\text{C}$  up to  $520^\circ\text{C}$  in a nitrogen atmosphere. Aqualabo Company UV-Visible line 9100 spectrophotometer that has a photometric range of 320-1100 nm. Other instruments are centrifuge, water bath sonicator and suction filtration assembly.

## 3.2 Methods

### 3.2.1 Preparation of graphite oxide

As shown in figure 8, graphite oxide was prepared by using the Hummers method, 1.0 g of graphite was grounded with 50.0 g of NaCl to reduce their dimensions, and then the mixture was dissolved in warm water, and stirred, filtrated, and dried in an oven 6 h. After that, the dry filtered graphite was mixed in 23 ml  $\text{H}_2\text{SO}_4$  with stirring, overnight. Therefore,

the mixture was put in an ice bath (below 10°C). 3.0 g of KMnO<sub>4</sub> was added slowly over 3 hours with stirring.

Afterward, the mixture was stirred for 30 min at 35±2°C, 45 min at 50±2°C, respectively. Then, 46 ml distilled water was added to the mixture and kept stirring at (98-105°C) for 45 min. The mixture was cooled down to room temperature and stirred with the addition of 140 ml D.W and 10 ml of 30% hydrogen peroxide H<sub>2</sub>O<sub>2</sub> to terminate the reaction. Mixture was filtered and washed five times with 5% HCl and D.W to remove any reaction by-product. After that, the graphite oxide was centrifuged (30 min, 5000 rpm) twice. Finally, a graphite oxide (final product) was placed in an oven to dry at 60°C for 6h [77].

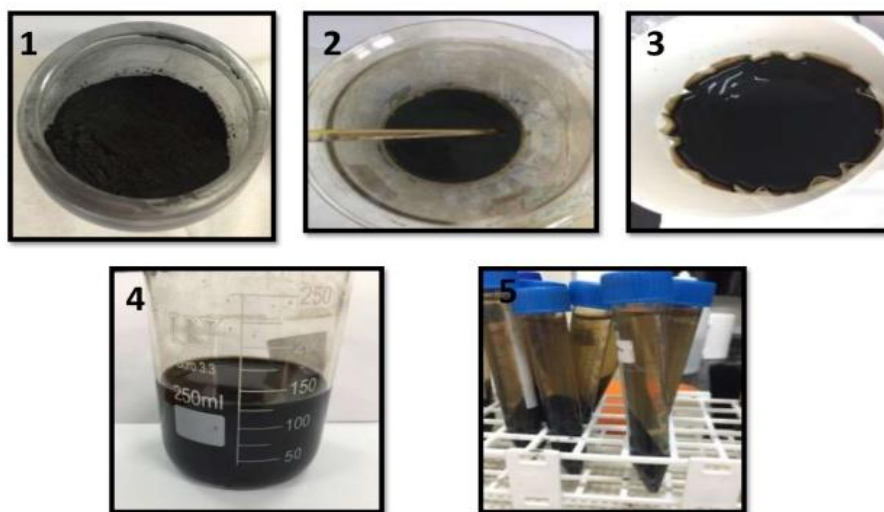


*Figure 8.* Preparation steps of graphite oxide

### 3.2.2 Preparation of graphene oxide nanoparticles

The graphite oxide ( 1.0 g / 200 ml D.W ) was added in tip sonicator for 30 min. Then, the mixture was centrifuged ( 1 hour , 6000 rpm ) [77].

### 3.2.3 Synthesis of iron oxide particles ( $\text{Fe}_3\text{O}_4$ ) (co-precipitation)

The solutions of iron (III) chloride hexahydrate and iron (II) sulfate heptahydrate were prepared by dissolving 0.270 g and 0.279 g respectively in 100 ml distilled water severally. Then the two solutions were mixed in a 250 ml round-bottom flask (twin – neck). After that 0.320 g of NaOH was added to the solution with stirred and heated to the temperature between 60-80°C for 6h. Afterward, the mixture was filtered by 0.45  $\mu\text{m}$  of filter paper, then washed five times with 0.3% HCl and distilled water. Lastly, the final product was dried in the oven at 60 °C [78].



*Figure 9.* Magnetic nanoparticle during preparation

### 3.2.4 Preparation of graphite oxide- $\text{Fe}_3\text{O}_4$ nanoparticles

25.0 mg of graphite oxide was added to 5.0 ml of DMF to exfoliate by water bath sonicator for 2 h at room temperature, and then the solution of 10 mg of  $\text{Fe}_3\text{O}_4$  in 5.0 ml of chloroform was added drop-wise into the graphite oxide solution. Afterward, the mixture was sonicated for 3 h at room temperature and the mixture of graphite oxide -  $\text{Fe}_3\text{O}_4$  was separated by centrifugation at 6000 rpm for 10 min twice. Finally, the final product was filtered and washed with hexane then distilled water several times [79].

### 3.2.5 Preparation of graphene oxide-Fe<sub>3</sub>O<sub>4</sub> nanoparticles

Graphene oxide –Fe<sub>3</sub>O<sub>4</sub> was prepared by liquid self-assembly method. Where 25.0 mg of GO was added to 5.0 ml of DMF to exfoliation by water bath sonicator for 2 h at room temperature, and then the solution of 10 mg of Fe<sub>3</sub>O<sub>4</sub> in 5.0 ml of chloroform was added dropwise into the GO dispersed. Afterward, the mixture was sonicated in water bath sonicator for 3 h at room temperature and the mixture of GO-Fe<sub>3</sub>O<sub>4</sub> was separated by centrifugation at 6000 rpm for 10 min twice. Finally, the final product was filtered and washed with hexane then distilled water several times [79].

### 3.2.6 Preparation of graphite oxide with chitosan

10 mg of graphite oxide was mixed with 20 mg of chitosan in an E-flask followed by adding 20 ml distilled water. The mixture was heated in a water bath (35-45)°C under magnetic stirring for 2 hours. The mixture was filtrated and dried in the oven at 40°C.

### 3.2.7 Preparation of graphene oxide with chitosan

10 mg of GO was mixed with 20 mg of chitosan in an E-flask, and followed by adding 20 ml distilled water. The mixture was heated in a water bath (35-45)°C under magnetic stirring for 2 hours. The mixture was filtrated and dried in the oven at 40°C.

### 3.2.8 Preparation of graphite oxide-chitosan-Fe<sub>3</sub>O<sub>4</sub> nanoparticles

10 mg of graphite oxide was mixed with 20 mg of chitosan in an E-flask. Afterward, 9 ml of distilled water was added to the mixture. The mixture was heated in a water bath at (35-45)°C under magnetic stirring for 2 hours. Thereafter, 1ml of iron oxide solution was added to the mixture. Then, the mixture was heated in a water bath (35-45) °c under magnetic stirring for 2 hours. Lastly, the mixture was filtrated and dried in the oven at 40°C.

### 3.2.9 Preparation of graphene oxide-chitosan-Fe<sub>3</sub>O<sub>4</sub> nanoparticles

10 mg of graphene oxide was mixed with 20 mg of chitosan in an E-flask. Afterward, 9 ml of distilled water was added to the mixture. The mixture was heated in a water bath at (35-45) °C under magnetic stirring for 2 hours. After that, 1 ml of iron oxide solution was added to the mixture. The mixture was heated in a water bath (35-45) °C under magnetic stirring for 2 hours. Lastly, the mixture was filtrated and dried in the oven at 40°C.

# **Chapter Four:**

## **Result and Discussion**

## 4.1 Characterization

Material characterization is an essential analytic method that uses a probe into the internal structure of materials to provide information on structure, mechanical, and magnetic characteristics.

### 4.1.1 Fourier-transform infrared spectroscopy (FT-IR)

The structure of GO-450 nm, GO-200 nm, Fe<sub>3</sub>O<sub>4</sub>, chitosan, GO/Fe<sub>3</sub>O<sub>4</sub> (two sizes), GO/Cs (two sizes) and GO/Cs/Fe<sub>3</sub>O<sub>4</sub> (two sizes) nanocomposites was analyzed by FT-IR spectroscopy.

#### I.FT-IR of Graphite, Graphite oxide-450nm, Graphene oxide-200nm

The spectra of graphite and graphite oxide as shown in figure 10(a,b) ensure the successful oxidation of graphite to graphite oxide. It can be noted the strong peak in graphite oxide at 3390 cm<sup>-1</sup> due to -OH stretching, and other peak in 1728 cm<sup>-1</sup> due to C-O (carboxyl) stretching and { CO-OH bending, C-OH stretching, and C-O stretching vibrations at 1357, 1223, 1056 cm<sup>-1</sup> }. The band at 1617 cm<sup>-1</sup> due to C=C [80].

As shown in figure 10(c) the spectrum of graphene oxide, the characteristic broad peak observed at 3645 cm<sup>-1</sup> is attributed to the -OH stretching vibration, the characteristic peak includes C=O stretching at 1936 cm<sup>-1</sup>, C=C stretching at 1836 cm<sup>-1</sup>, and C-O stretching at 1275 cm<sup>-1</sup>.

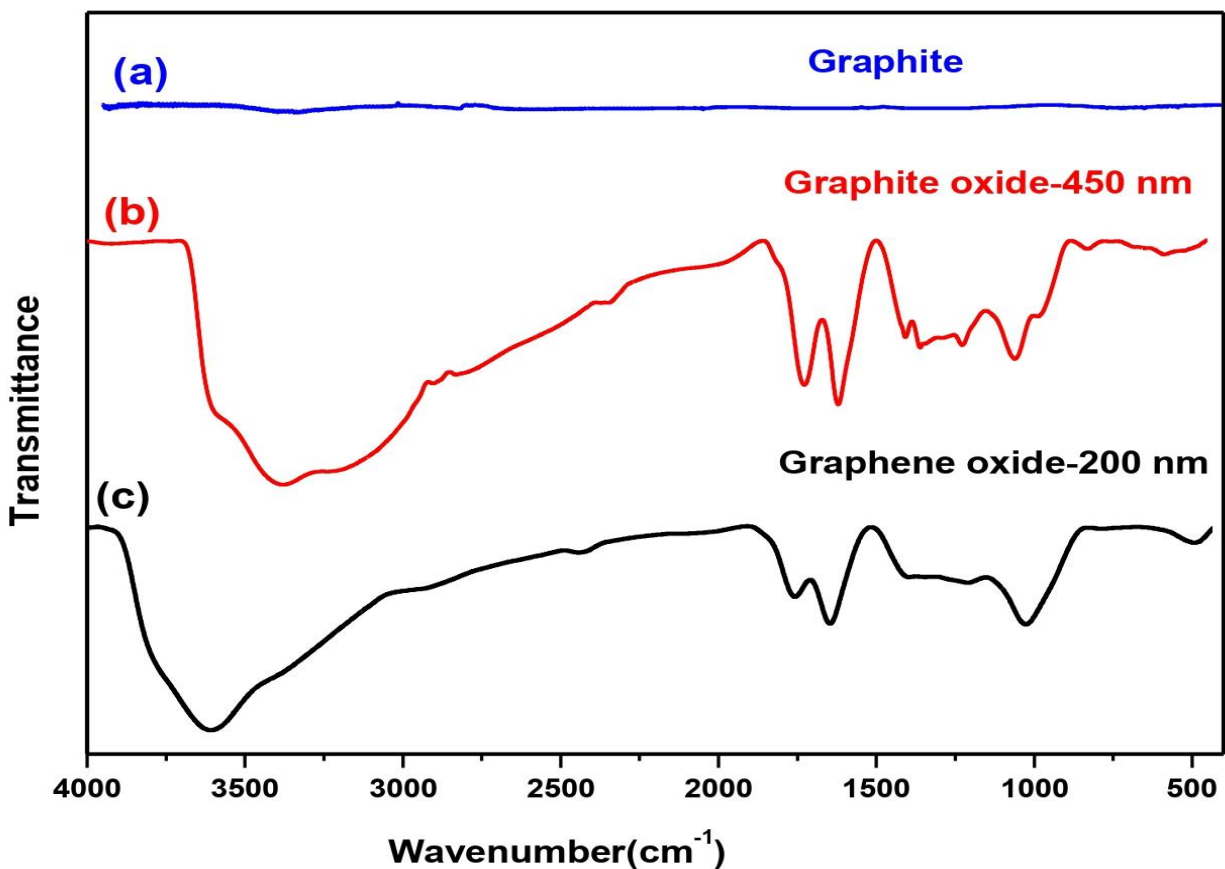


*Figure 10.* FT-IR spectra of (a) graphite, (b) graphite oxide and (c) graphene oxide .

## II. FT-IR of Fe<sub>3</sub>O<sub>4</sub>

The FT-IR spectrum of prepared Fe<sub>3</sub>O<sub>4</sub> nanoparticles are shown in figure 11. A strong peak at around 576 cm<sup>-1</sup> can be attributed to the Fe—O—Fe stretching vibration [81]. The broad band at around 3342 cm<sup>-1</sup> and the peak at 1619 cm<sup>-1</sup> are due to the adsorbed OH groups (comes from water).

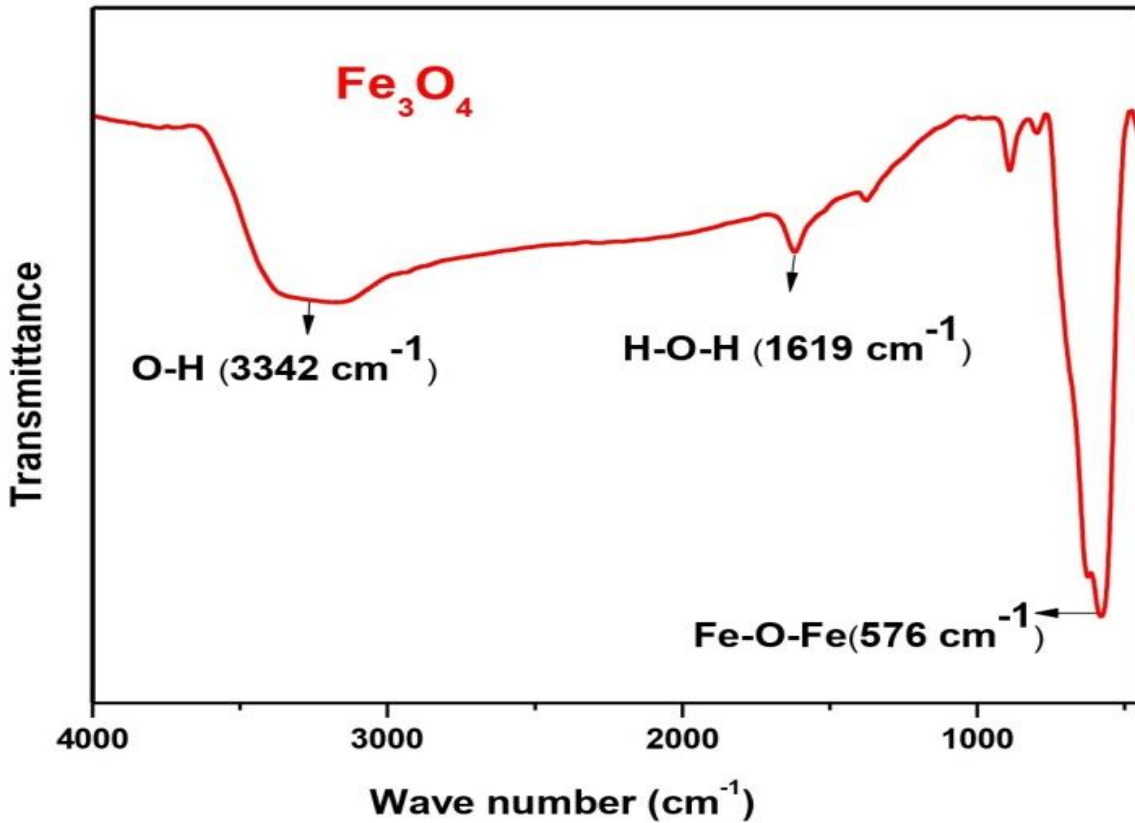


*Figure 11.* FT-IR spectrum of  $\text{Fe}_3\text{O}_4$ .

### III. FT-IR of (GO-450 nm / $\text{Fe}_3\text{O}_4$ ) and (GO-200 nm / $\text{Fe}_3\text{O}_4$ )

Figure 12 (a) exhibits the IR spectrum GO-450 nm /  $\text{Fe}_3\text{O}_4$  spectrum shows a characteristic peak at  $588 \text{ cm}^{-1}$  that was attributed to Fe-O, confirming the existence of  $\text{Fe}_3\text{O}_4$ , and shows a new strong peak at  $1382 \text{ cm}^{-1}$  due to formation of C-F bond [82].

In FT-IR spectrum of GO-200 nm as shown in figure (10,c), While GO-200 nm /  $\text{Fe}_3\text{O}_4$  shows a new peak at  $1398 \text{ cm}^{-1}$  due to formation C-F bond.

When compared between two spectra (figure 10,c and figure 12,b ) show a shift in the OH-peak from  $3645 \text{ cm}^{-1}$  to  $3451 \text{ cm}^{-1}$  also shift in the C=O (carboxylic acid function group) from  $1836 \text{ cm}^{-1}$  to  $1789 \text{ cm}^{-1}$  due to the formation of -COO- after  $\text{Fe}_3\text{O}_4$  nanoparticles are bonded presented. Furthermore, the presence of  $\text{Fe}_3\text{O}_4$  nanoparticles in GO-200 /  $\text{Fe}_3\text{O}_4$  composite is ensured from the peak observed at  $568 \text{ cm}^{-1}$ , owing to the Fe-O stretching mode [83].

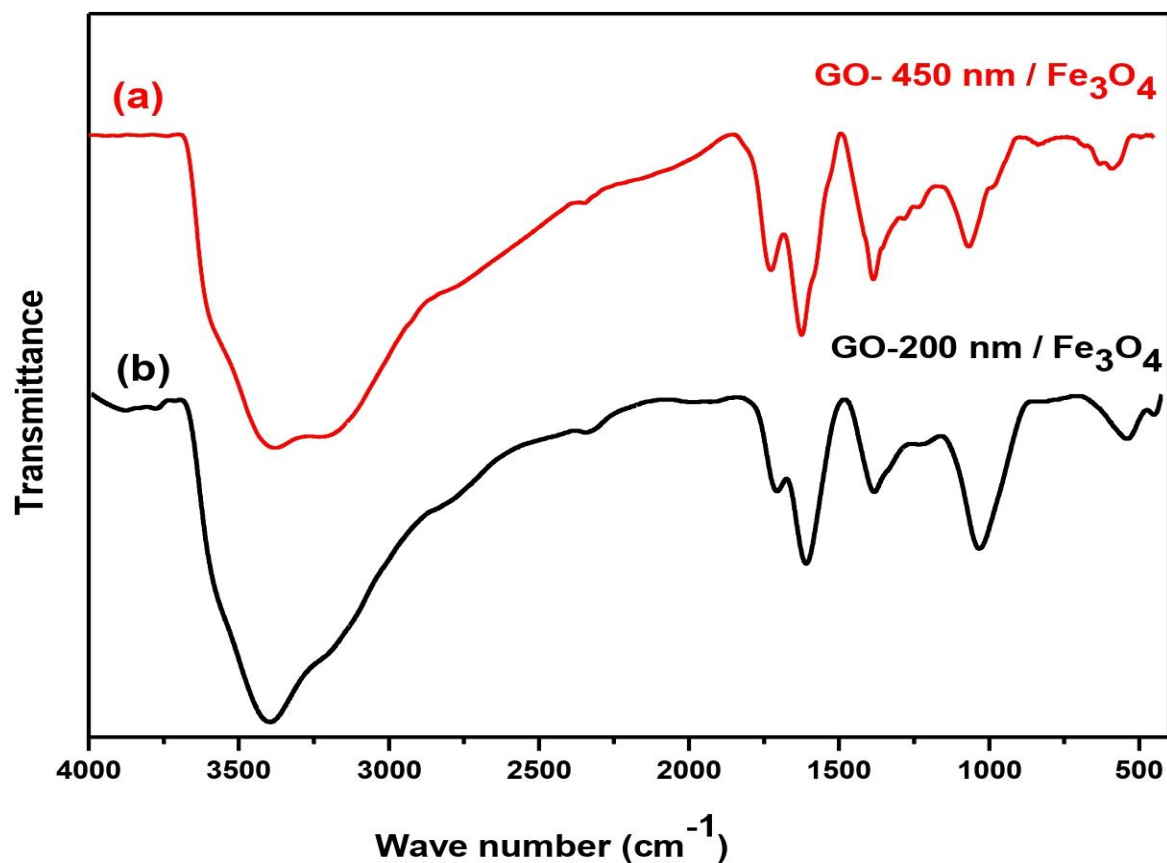


*Figure 12.* FT-IR of spectra of (a) GO-450 nm/Fe<sub>3</sub>O<sub>4</sub>, (b) GO-200 nm/Fe<sub>3</sub>O<sub>4</sub>.

#### IV. FT-IR of chitosan

The chitosan containing many function groups like hydroxyl, carboxyl, carbonyl, amid and amine. The presence of these groups make the chitosan able to form bonds between the chitosan chain and the sheet of graphite oxide.

As show in figure 13, the broad peak at 3404 cm<sup>-1</sup> corresponds to N-H and O-H stretching. The C-H symmetrical and asymmetric were definite by the peaks at 2882 cm<sup>-1</sup> and 2119 cm<sup>-1</sup>. The presence of N-acetyl group was definite by the peak at around 1659 cm<sup>-1</sup> (C=O stretching of amide 1 ) and 1315 cm<sup>-1</sup> (C-N stretching of amide 3 ). The peaks at 1588 cm<sup>-1</sup> and 1378 cm<sup>-1</sup> corresponds to N-H bending of primary amine and CH<sub>3</sub> symmetrical, respectively. The peak at 1081 cm<sup>-1</sup> and 600 cm<sup>-1</sup> refer to C-O-C asymmetric stretching bridge and C-H bending out of the plane, respectively [84],[85].

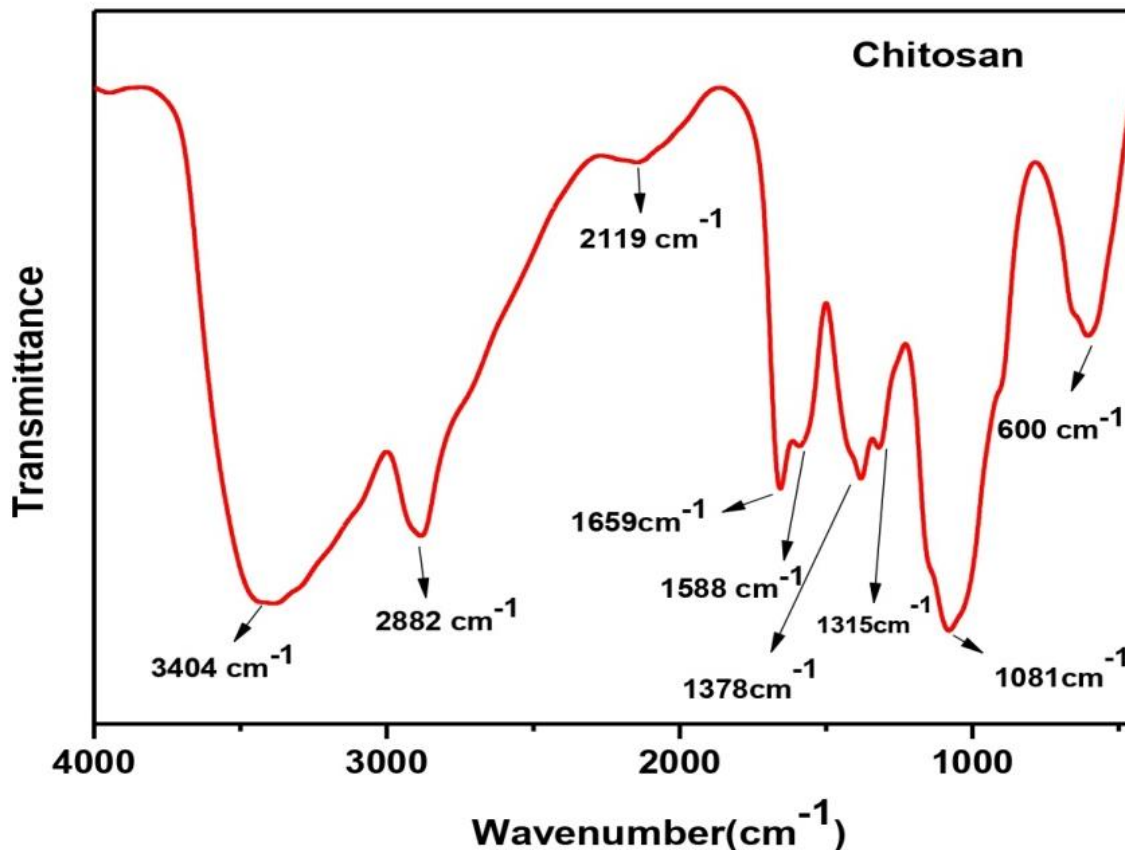


*Figure 13.* FT-IR spectra of chitosan.

#### V. FT-IR of GO-450 nm /Cs and GO-200 nm /Cs

The FT-IR spectrum of GO-450 nm / Cs is shown in figure (14,a), the identical bands that of the chitosan and GO-450 nm such as the broad peaks at  $3404\text{ cm}^{-1}$  are assigned to the OH groups in GO-450 nm and the amine stretch in chitosan.

The intensity of the peak at  $1085\text{ cm}^{-1}$  (C-O stretching vibration) increased compared to GO-450 nm, due to the van der waals forces. In the other side, the peak at  $1628\text{ cm}^{-1}$  is assigned to the COOH group from GO-450 nm (figure 10,b) and is downshifted because of hydrogen bonding between GO-450 nm and hexatomic ring of chitosan.

The peak at  $1390\text{ cm}^{-1}$  is assigned to the C=C group from GO-450 nm, GO-450 nm spectrum the peak of C=C group appeared at  $1615\text{ cm}^{-1}$  and is downshifted compared to original GO-450 nm. Finally, the peak at  $1085\text{ cm}^{-1}$  is assigned to C-O-C stretching in the

GO-450 nm. The FT-IR results improved the presence of physical forces between GO-450 nm and chitosan [86].

In figure (14,b) the spectrum of GO-200 nm / chitosan shows a group of characteristics identical to that of the chitosan and GO-200 nm such as the peak at  $2960\text{ cm}^{-1}$  which can be fixed to the C-H asymmetric vibration. The new peak appeared at  $1530\text{ cm}^{-1}$  due to the C=C stretching. When GO-200 nm was mixed with chitosan the absorption peak at  $3349\text{ cm}^{-1}$  was broadened and downshifted from  $3650\text{ cm}^{-1}$  in GO-200 nm spectrum. The intensity of the peak at  $1242\text{ cm}^{-1}$  (C-O stretching vibration) was increased, finally the peak at  $1783\text{ cm}^{-1}$  is assigned to the C=O group from graphene oxide (in spectrum of GO-200 nm the peak of C=C group appeared at  $1838\text{ cm}^{-1}$ ) and is downshifted compared to GO-200 nm spectrum [87].

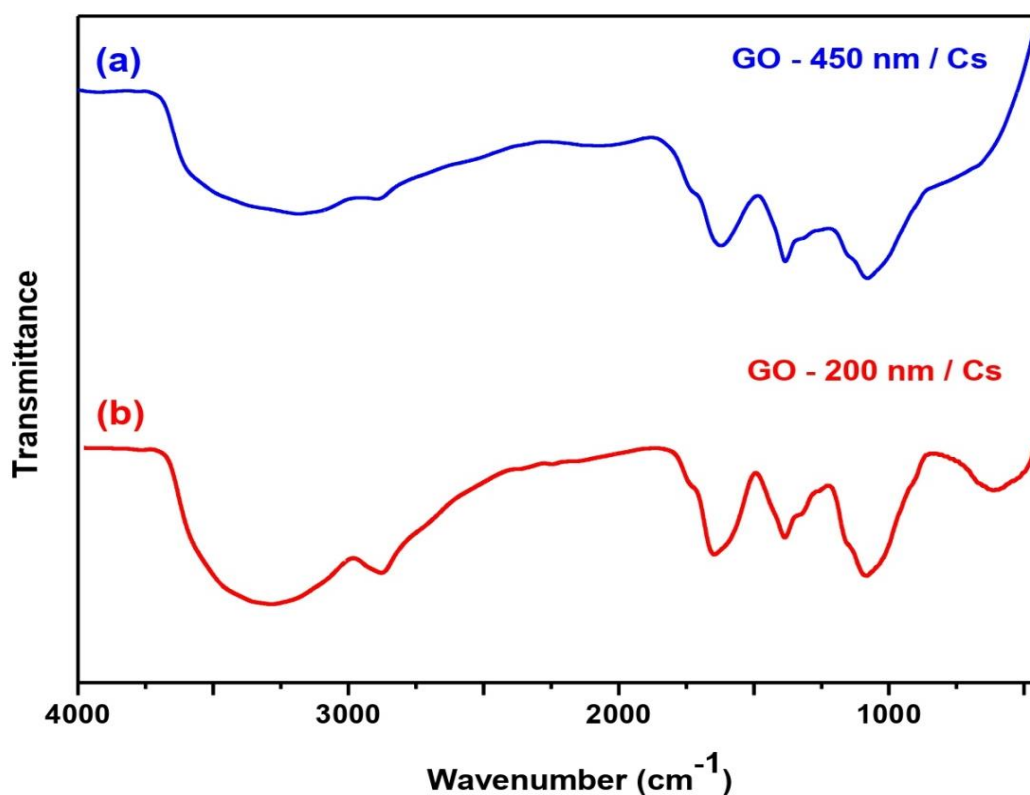


*Figure 14.* FT-IR spectra of (a)GO-450 nm /Cs and (b) GO-200 nm / Cs .

## VI.FT-IR of GO-450 nm / Cs / Fe<sub>3</sub>O<sub>4</sub> and GO-200nm / Cs / Fe<sub>3</sub>O<sub>4</sub>

In figure (15,a) the spectrum of GO-450 nm/Cs/Fe<sub>3</sub>O<sub>4</sub> showed the characteristic peak of O-H at 3310 cm<sup>-1</sup>. When compared the spectrum of GO-450 nm/Cs ( figure14,a) and GO-450 nm/Cs/Fe<sub>3</sub>O<sub>4</sub> the same peaks. However GO-450 nm/Cs/Fe<sub>3</sub>O<sub>4</sub> showed a new peak at 570 cm<sup>-1</sup> that was attributed to Fe-O, this peak confirms the attachment of iron oxide particles with GO-450 nm/Cs [88].

In figure (15,b) the spectrum of GO-200 nm/Cs/Fe<sub>3</sub>O<sub>4</sub> showed the characteristic peaks of O-H at 3290 cm<sup>-1</sup>. When compared between the spectrum of GO-200 nm /Cs (figure 14,b) and GO-200 nm/Cs/Fe<sub>3</sub>O<sub>4</sub> have the same peak. However GO-200 nm/Cs/Fe<sub>3</sub>O<sub>4</sub> showed peak with more sharp and a peak at 650 cm<sup>-1</sup> that was attributed to Fe-O, this peak confirms the attachment of iron oxide particles with GO-200 nm/Cs [88] .

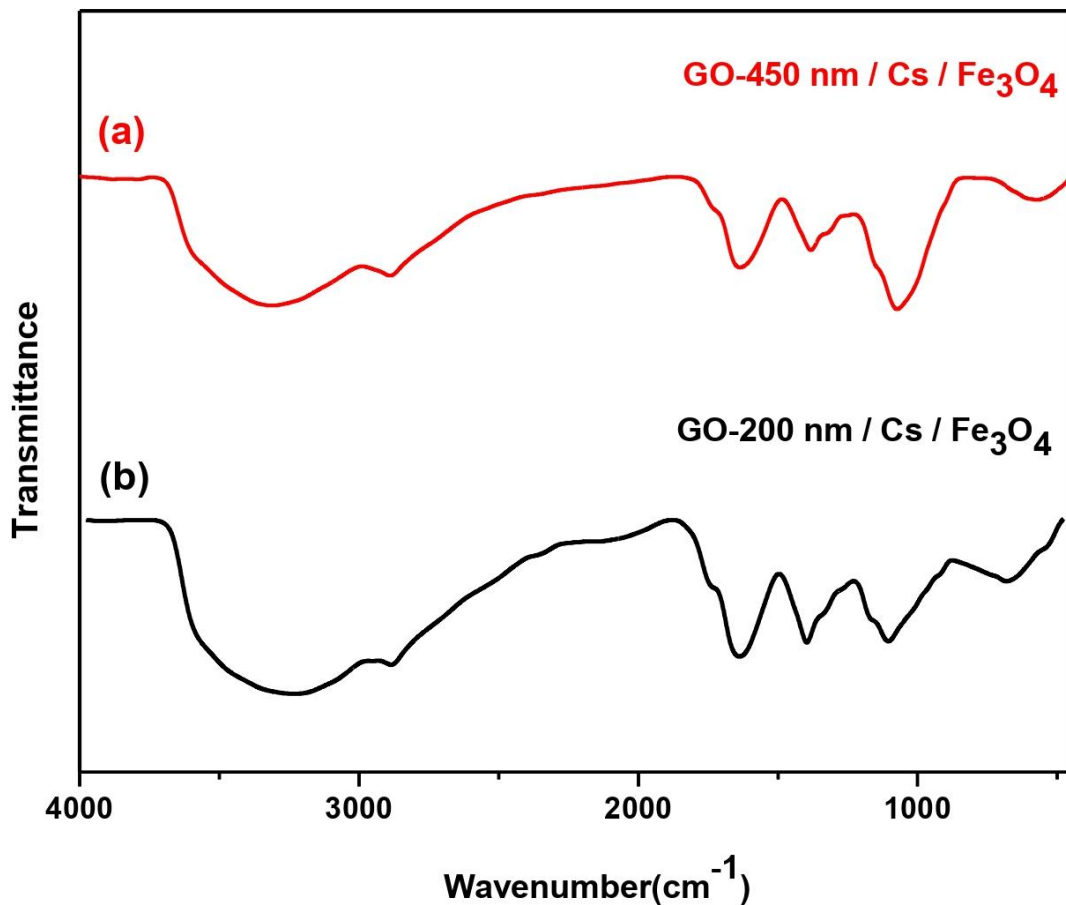


*Figure 15.* spectra of (a) GO-450 nm/Cs/Fe<sub>3</sub>O<sub>4</sub> and (b) GO-200 nm/Cs/Fe<sub>3</sub>O<sub>4</sub>.

## 4.1.2 UV-visible spectrophotometer study

### I. UV-visible spectroscopy of iron oxide particles

The UV-Vis absorption spectrum of prepared  $\text{Fe}_3\text{O}_4$  particles show the maximum absorption around 219 nm in figure 17, due to both absorption and scattering of UV-Visible radiation by the magnetic particles [89].

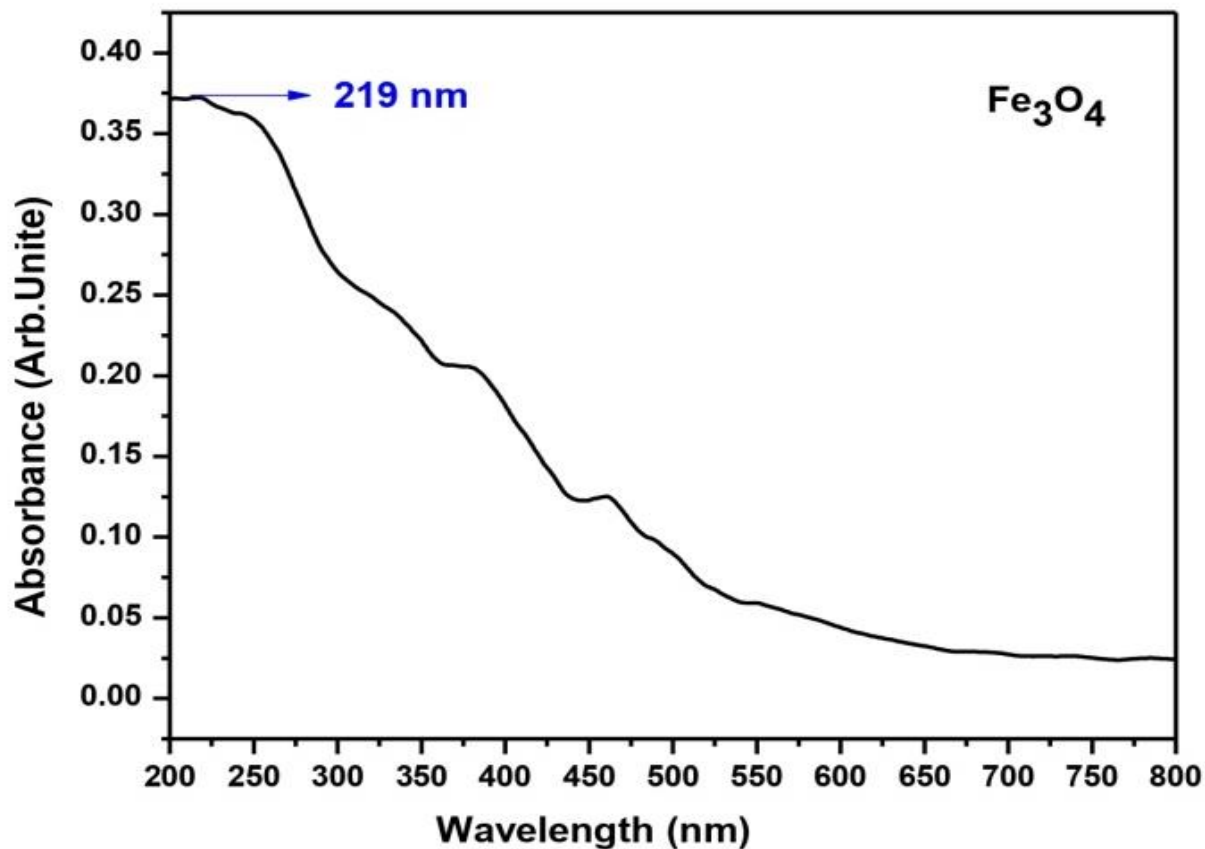


*Figure 17.* UV-Vis spectrum of  $\text{Fe}_3\text{O}_4$  .

## II. UV-visible of GO-450 nm and GO-200 nm

The UV-Vis spectrum of GO-450 nm shows a single absorption peak at 275 nm as displayed in figure 18, which attributed to  $\pi \rightarrow \pi^*$  transition of the aromatic C=C bonds, and GO-200 nm presented strong absorption peak at 238 nm corresponding to  $\pi \rightarrow \pi^*$  transitions of aromatic C – C bond [90] .

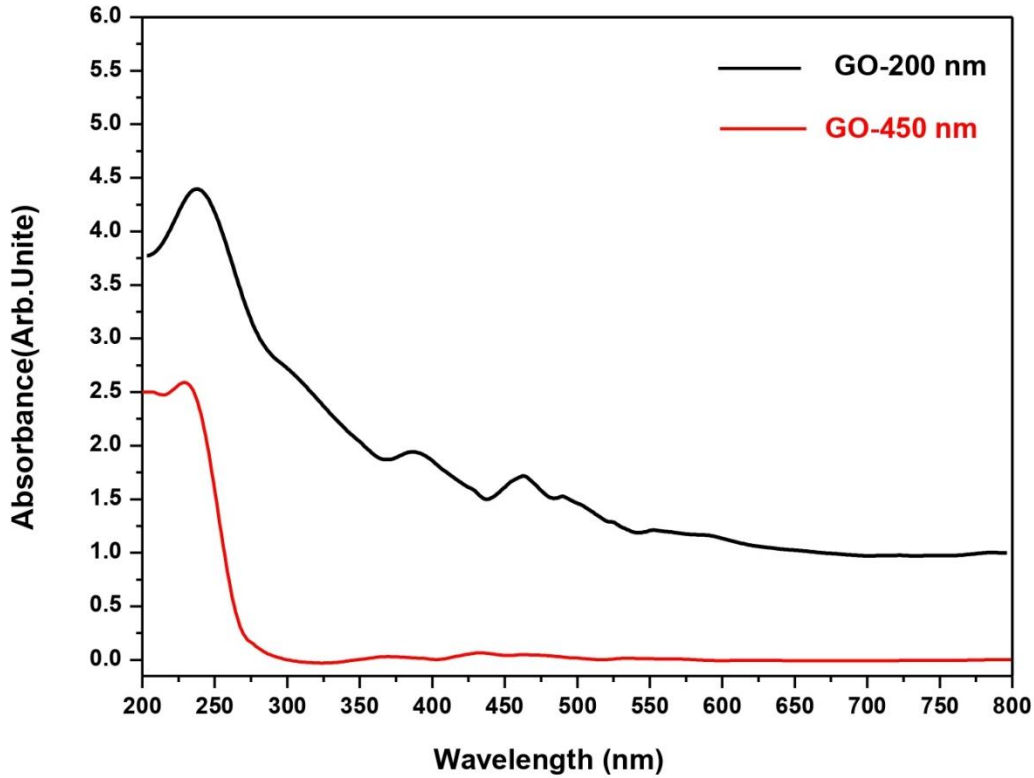


*Figure 18.* UV-Vis spectra of GO-450 nm and GO-200 nm.

## III. UV-visible of GO-450 nm / Fe<sub>3</sub>O<sub>4</sub> and GO-200 nm / Fe<sub>3</sub>O<sub>4</sub>

The presence of Fe<sub>3</sub>O<sub>4</sub> in GO-450 nm composite is ensured from the UV-Vis spectrum as shown in figure 19, GO-450 nm / Fe<sub>3</sub>O<sub>4</sub> spectrum the absorption peak blueshifted to 255 nm (compared to GO-450 nm spectrum in figure 18 ), because the Fe<sub>3</sub>O<sub>4</sub> distributed on GO-450 nm surface. While for GO-200 nm / Fe<sub>3</sub>O<sub>4</sub> the absorption peak redshifted to 278 nm ( compared to GO-200 nm spectrum in figure 18 ), because the attachment of Fe<sub>3</sub>O<sub>4</sub> on GO-200 nm surface [91].

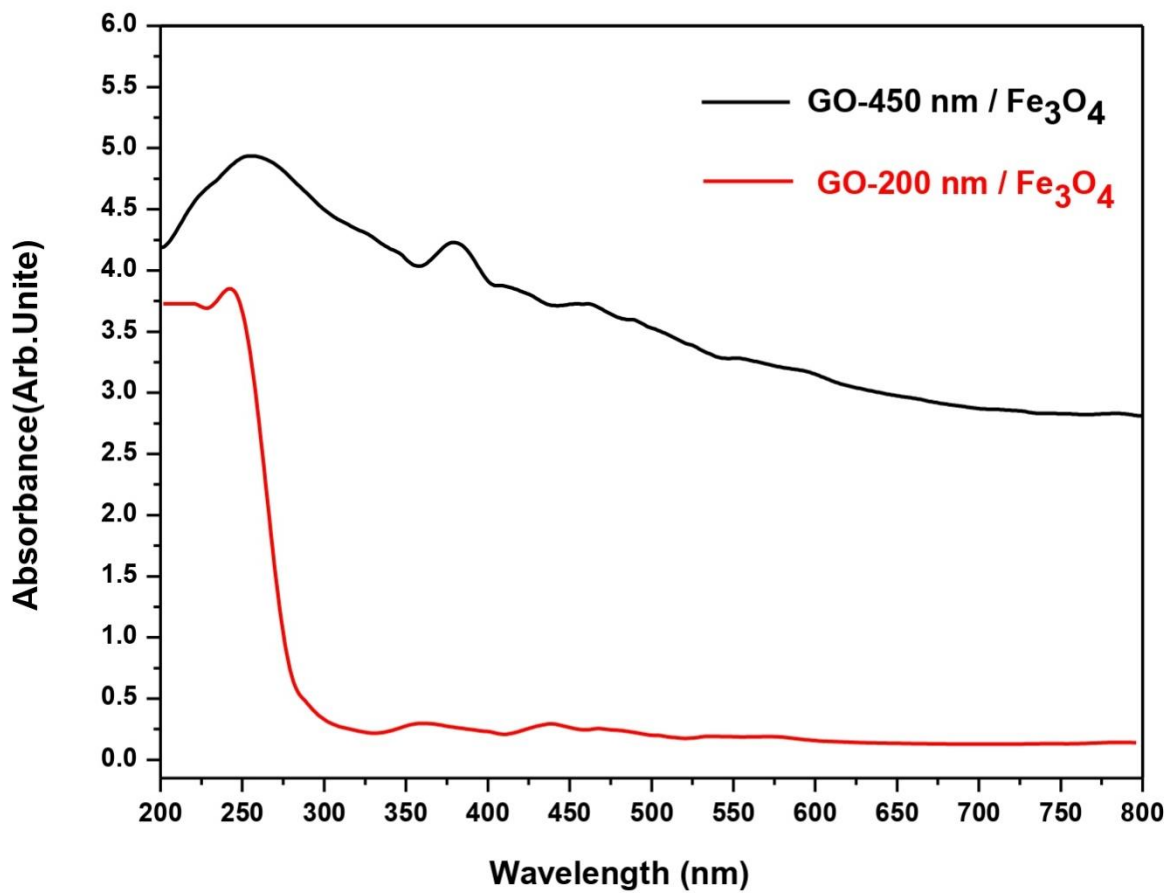


*Figure 19.* UV-Vis spectra of GO-450 nm / Fe<sub>3</sub>O<sub>4</sub> and GO-200 nm / Fe<sub>3</sub>O<sub>4</sub>.



*Figure 20.* The separation and redispersion of a solution of GO-200 nm / Fe<sub>3</sub>O<sub>4</sub> in the absence (left) and presence of an external magnetic field (right) .

#### IV. UV-visible of chitosan

The optical properties of chitosan was analysis by UV-Vis spectroscopy. The chitosan spectrum showed a peak at 209 nm as shown in figure 21 that can be due to chitosan composed of two types of monomer D-glucosamine and N-acetyl-D-glucosamine so the  $n \rightarrow \pi^*$  electron transition. These transitions are attributed to the C=O of the N-acetyl group in chitosan [86].

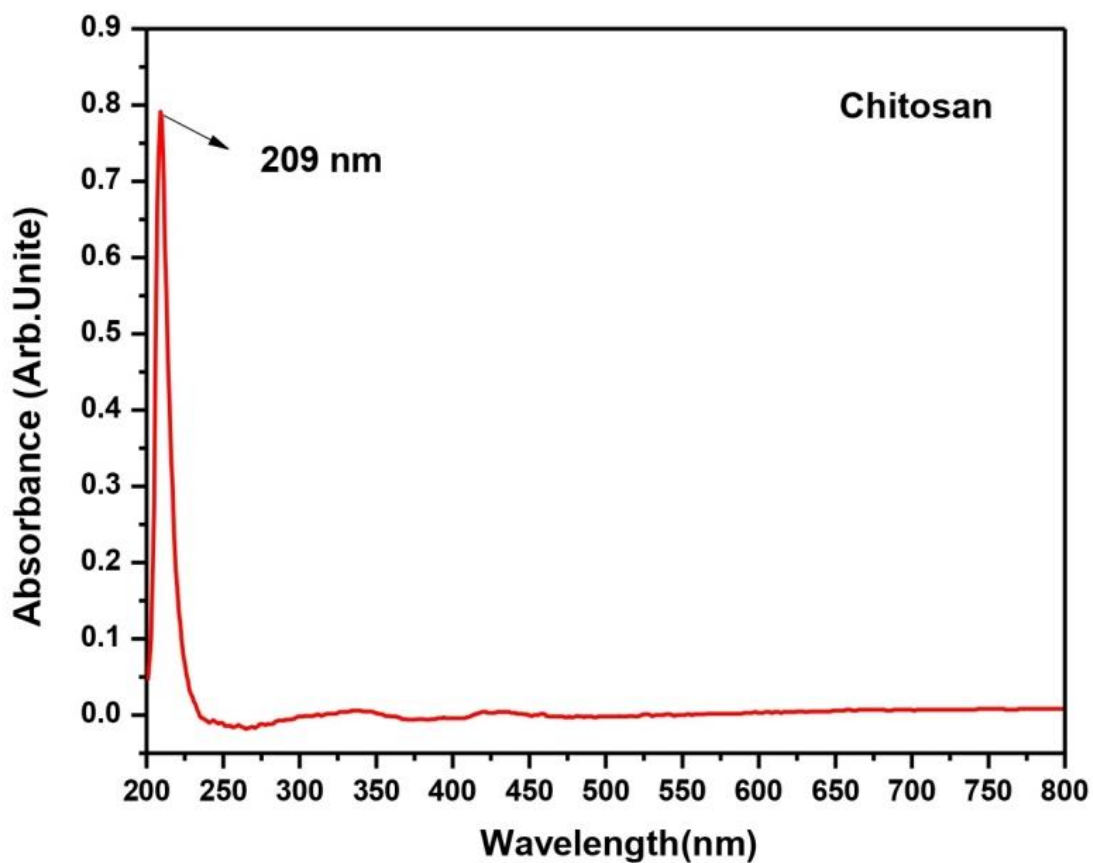


*Figure 21.* UV-Vis spectrum of chitosan.

## V. UV-visible of GO-450 nm / Cs and GO-200 nm / Cs

The UV-Vis spectrum of GO-450 nm / Cs in figure 22 show the absorption peak blueshifted to 208 nm (compared to GO-450 nm spectrum in figure 18 ), because of the interaction between chitosan and GO-450 nm [92], but in spectrum of GO-200 nm / chitosan, the peak at 238 nm of GO-200 nm was redshifted to 248 nm due to the interaction between GO-200 nm and chitosan [92].

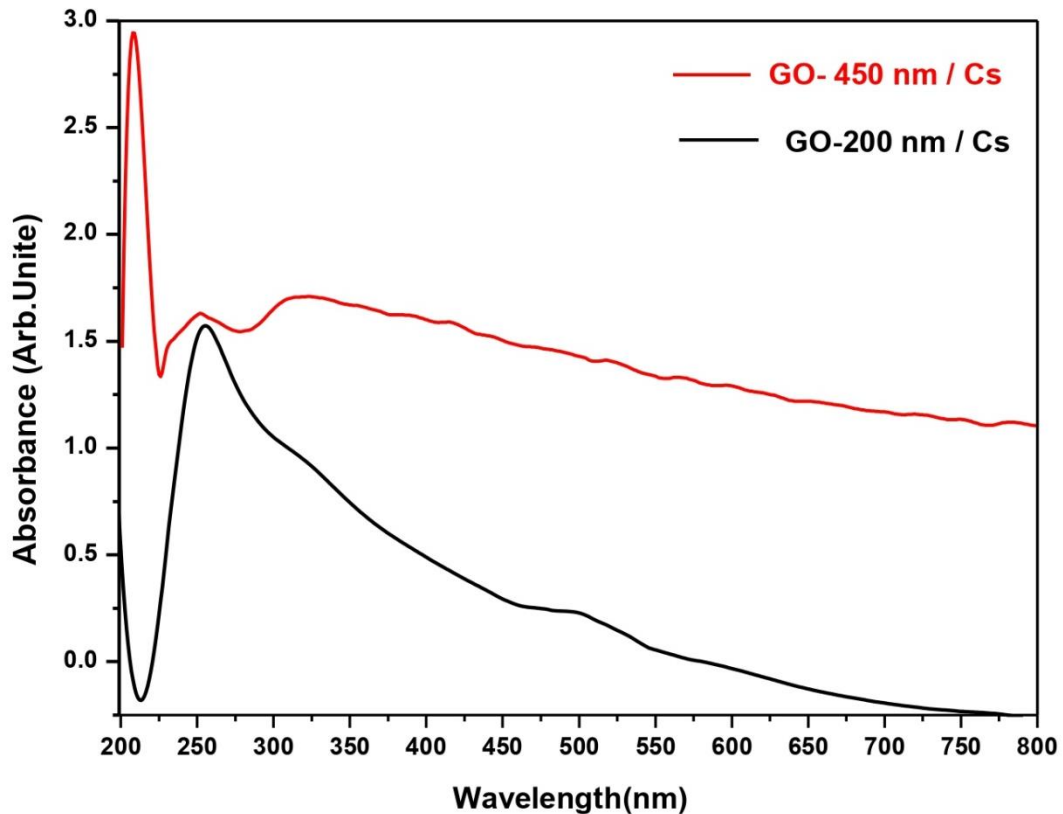


*Figure 22.* UV-Vis spectra of GO- 450 nm / Cs and GO-200 nm / Cs .

## VI. UV-visible of GO-450 nm/Cs/Fe<sub>3</sub>O<sub>4</sub> and GO-200 nm/Cs/Fe<sub>3</sub>O<sub>4</sub>

The UV-Vis spectrum of GO-450 nm /Cs in figure 22 shown a single absorption peak at 208 nm. While for GO-450 nm /Cs/Fe<sub>3</sub>O<sub>4</sub> the absorption peak redshifted to 238 nm as shown in figure 23, because of the interaction between Fe<sub>3</sub>O<sub>4</sub> and GO-450 nm /Cs also the maximum wavelength for iron oxide was 219 nm so the shifted in GO-450 nm /Cs spectrum was redshifted.

In other hand, spectrum of GO-200 nm/Cs shown a peak at 248 nm in figure 22, but in spectrum of GO-200 nm/Cs/Fe<sub>3</sub>O<sub>4</sub>, the peak of GO-200 nm/Cs was blueshifted to 240 nm indicating to the interaction between Fe<sub>3</sub>O<sub>4</sub> and GO-200 nm/Cs.

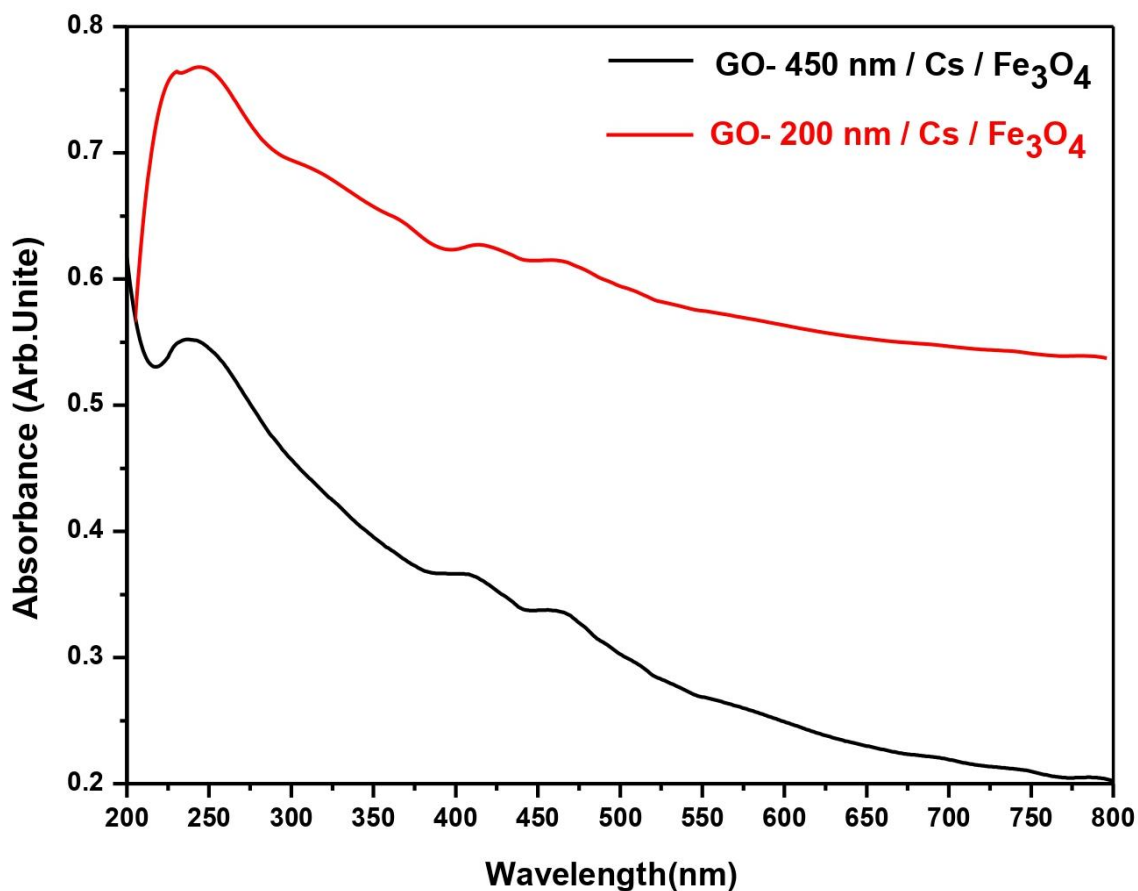
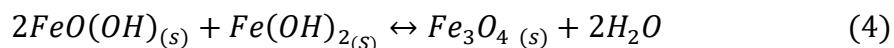
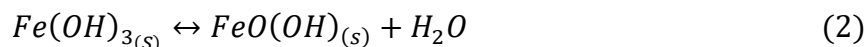


*Figure 23.* UV-Vis spectra of GO-450 nm/Cs/Fe<sub>3</sub>O<sub>4</sub> and GO-200 nm/Cs/Fe<sub>3</sub>O<sub>4</sub>.

### 4.1.3 Synthesis of Fe<sub>3</sub>O<sub>4</sub>

Fe<sub>3</sub>O<sub>4</sub> were prepared by co-precipitation method from the reaction of FeCl<sub>3</sub>.6H<sub>2</sub>O and FeSO<sub>4</sub>.7H<sub>2</sub>O in sodium hydroxide solution. The proposed mechanism of Fe<sub>3</sub>O<sub>4</sub> preparation is as followed.



The net reaction :  $2Fe^{+3} + Fe^{+2} + 8OH^{-} \leftrightarrow Fe_3O_4(s) + 4H_2O$

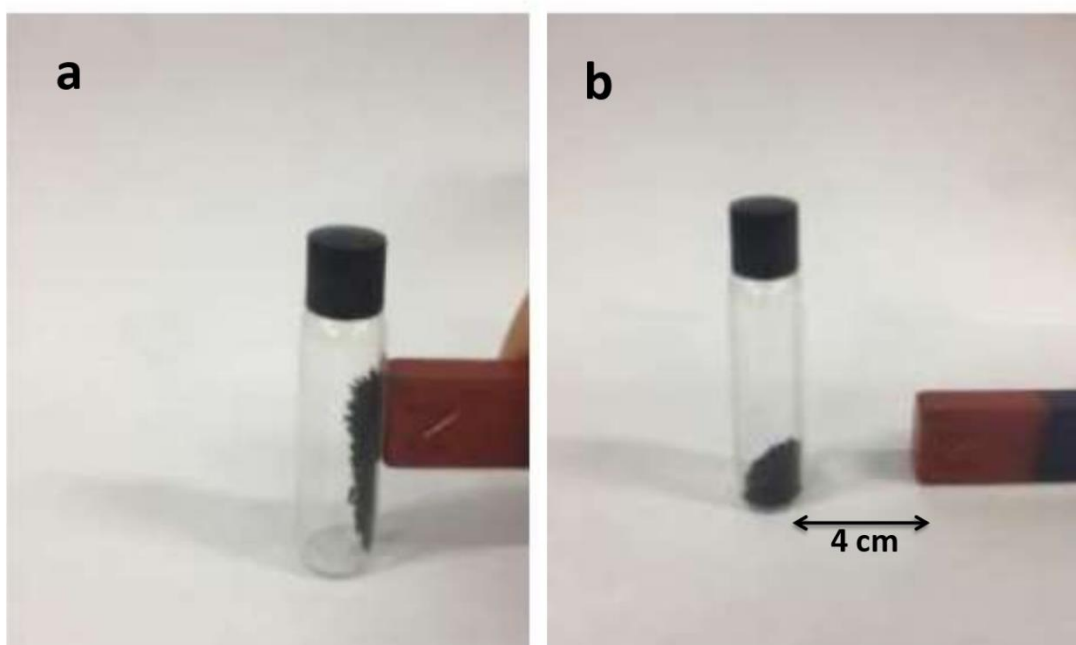


**Figure 24.** Magnetic activity of  $Fe_3O_4$  particles with (a) and without external magnetic field (b).

#### 4.1.4 Differential scanning calorimetry (DSC)

Differential Scanning Calorimetry (DSC) is most thermal analysis technique. It measures endothermic and exothermic transition as a function of temperature. The DSC thermographs of  $Fe_3O_4$ , GO-200 nm and GO-200 nm /  $Fe_3O_4$  are shown in figure 25, 26 and 27 respectively.

The DSC of pure  $Fe_3O_4$  was showed a endothermic peak at  $100^{\circ}C$ , due to removal of the solvent molecule ( $H_2O$ ). The region between  $(100-400)^{\circ}C$  have no thermal change

[93], due to high chemical stability of  $\text{Fe}_3\text{O}_4$ , therefore no thermal transition will appear in the range of GO studied.

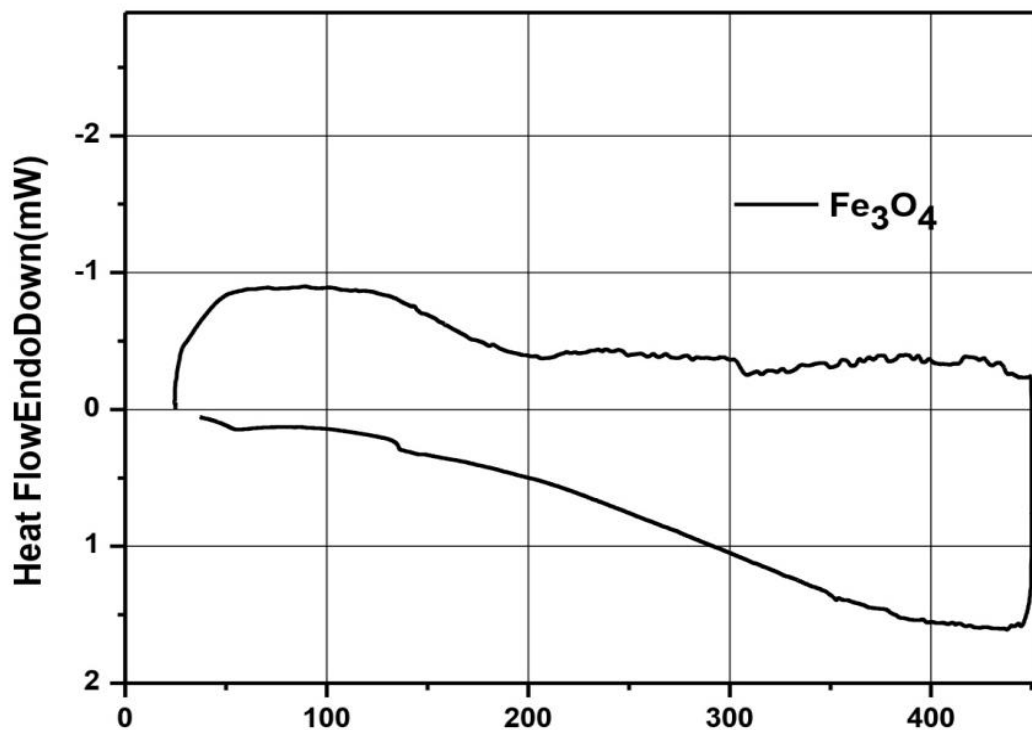


*Figure 25.* DSC thermal study of  $\text{Fe}_3\text{O}_4$ .

The DSC of pure GO-200 nm was showed a endothermic peak in the region below 100 °C due to loss of  $\text{H}_2\text{O}$  molecule in GO-200 nm, and another exothermic peak appears around 200 °C due to the thermal decomposition of unstable oxygen-containing function groups because of pyrolysis of oxygenated functional group such as hydroxyl, carbonyl and carboxylic acid to yield  $\text{CO}$ ,  $\text{CO}_2$  and  $\text{H}_2\text{O}$  [94].

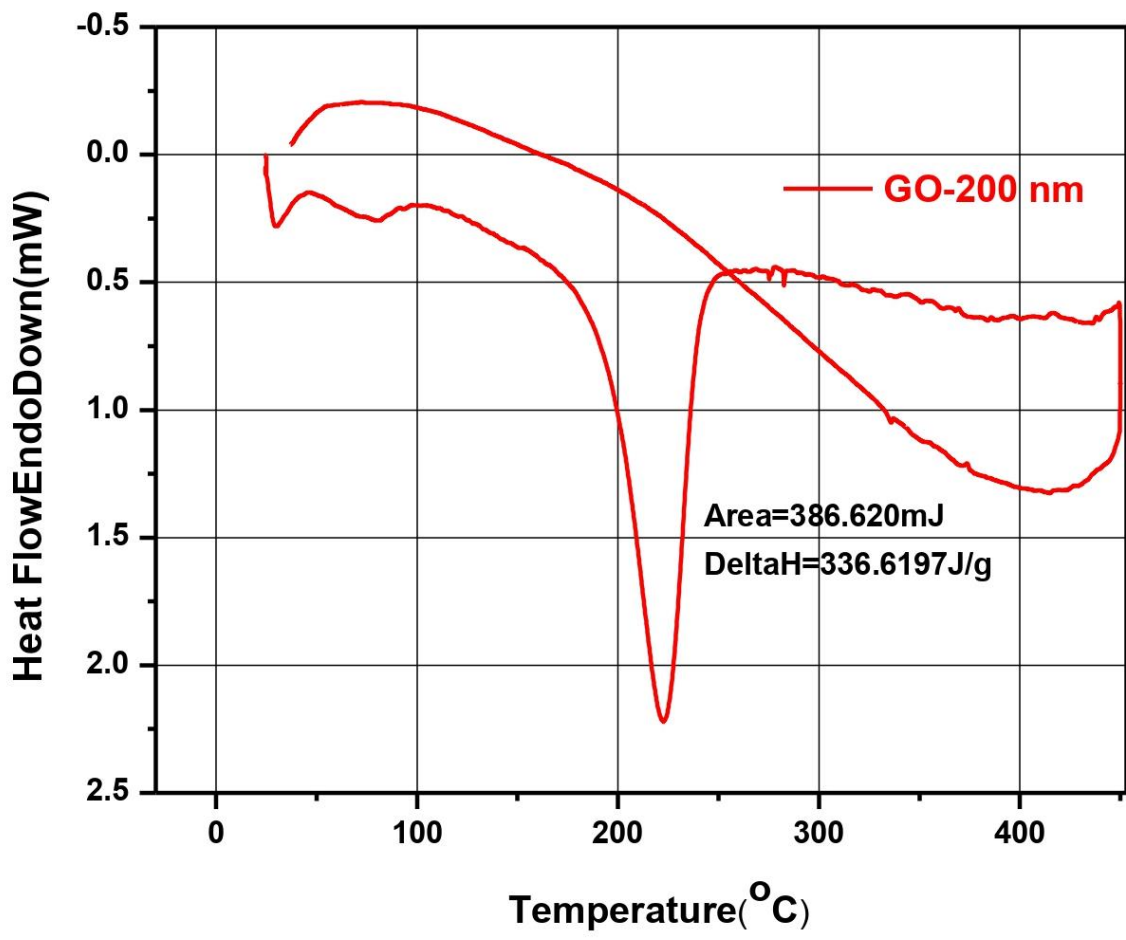


*Figure 26.* DSC thermal study of GO-200 nm .

Finally, the DSC of GO-200 nm / Fe<sub>3</sub>O<sub>4</sub> are shown a exothermic peak at 223 °C have the same position of exothermic peak in GO-200 nm thermograph but with different area under the peak (area = 1662 \* 10<sup>-3</sup> J ) due to interaction between GO-200 nm and Fe<sub>3</sub>O<sub>4</sub> and it can be fixed to the decomposition of carbon skeleton, another strong endothermic peak appears at 59.89 °C due to the decay interaction between GO-200 nm and Fe<sub>3</sub>O<sub>4</sub> [94].

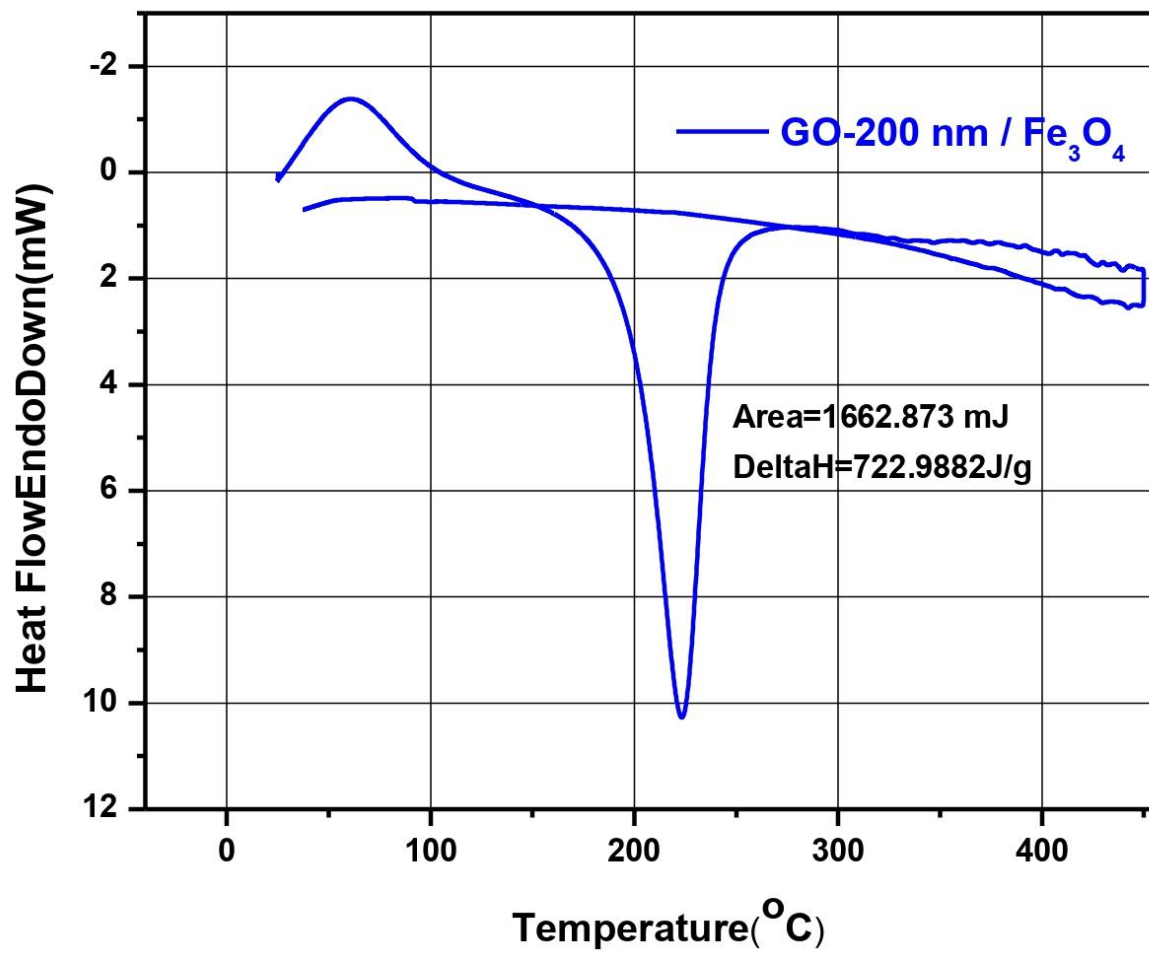


*Figure 27.* DSC thermal study of GO-200 nm / Fe<sub>3</sub>O<sub>4</sub> .

# **Chapter Five:**

# **Conclusion and**

# **Recommendations**

## 1.1 Conclusion

The present study successfully created a simple, efficient, cost-effective, and environmentally friendly process for producing magnetic iron oxide particles, two sizes of GO, and magnetically separable GO/Cs/Fe<sub>3</sub>O<sub>4</sub> nanoparticles.

## 1.2 Recommendations

The GO/Cs/Fe<sub>3</sub>O<sub>4</sub> nanocomposite is appropriate for the creation of tailored drug delivery for various cancer cells.

In future research, drug will be added to a nanocomposite of GO/ Cs/ Fe<sub>3</sub>O<sub>4</sub>, and the system will be tested on normal cell lines to see how effective the drug system is and how it affects cancer cells.

## References

- [1] A. R. Wu and L. Yu, “There’s plenty of room at the bottom of a cell,” *Chem. Eng. Prog.*, vol. 113, no. 10, 2017.
- [2] L. Leon, E. J. Chung, and C. Rinaldi, “A brief history of nanotechnology and introduction to nanoparticles for biomedical applications.” Elsevier Inc., 2019.
- [3] S. Ghorai, “Chemical, physical and mechanical properties of nanomaterials and its applications., PhD (Doctor of Philosophy) thesis,” Univ. Iowa, p. 166, 2013.
- [4] S. Khare, K. Williams, and K. Gokulan, “Nanotechnology, ” 1 st Editi. 2014.
- [5] Mihail C. Roco . Chad A. Mirkin . Mark C.Hersam, “Nanotechnology research directions for societal needs in 2020. ” 2020.
- [6] H. Fatima, T. Charinpanitkul, and K.-S. Kim, “Fundamentals to apply magnetic nanoparticles for hyperthermia therapy,” *Nanomaterials*, vol. 11, no. 5, p. 1203, 2021.
- [7] Y. Cui, Q. Wei, H. Park, and C. M. Lieber, “Nanowire nanosensors for highly sensitive and selective detection of biological and chemical species,” *Science*, vol. 293, no. 5533, pp. 1289–1292, 2001.
- [8] Y. L. Bunimovich, G. Ge, K. C. Beverly, R. S. Ries, L. Hood, and J. R. Heath, “Electrochemically programmed, spatially selective biofunctionalization of silicon wires,” *Langmuir*, vol. 20, no. 24, pp. 10630–10638, 2004.
- [9] R. J. Chen et al., “Noncovalent functionalization of carbon nanotubes for highly specific electronic biosensors,” *Proc. Natl. Acad. Sci. U. S. A.*, vol. 100, no. 9, pp. 4984–4989, 2003.
- [10] P. Rychahou et al., “Colorectal cancer lung metastasis treatment with polymer–drug nanoparticles,” *J. Control. Release*, vol. 275, pp. 85–91, 2018.
- [11] Ananya Deb and R. Vimala, “Camptothecin loaded graphene oxide nanoparticle functionalized with polyethylene glycol and folic acid for anticancer drug delivery,” *J. Drug Deliv. Sci. Technol.*, vol. 43, no. October 2017, pp. 333–342, 2018.
- [12] X. Zhang and C. Xiao, “Biofabrication of silver nanoparticles and their combined effect with low intensity ultrasound for treatment of lung cancer,” *J. Photochem. Photobiol. B Biol.*, vol. 181, no. 2017, pp. 122–126, 2018.
- [13] Tsai-Jung Wu , Hsiao-Yu Chiu , John Yu, “Nanotechnologies for early diagnosis, in situ disease monitoring, and prevention. ”, pp.1-92, 2018.

- [14] A. Krueger, "Carbon – element of many faces," in Carbon Materials and Nanotechnology, pp. 1–32, 2010.
- [15] I. Carbon, G. Iv, and P. Table, "Introduction to carbon materials 1.1," no. c, pp. 1–19.
- [16] O. Zaytseva and G. Neumann, "Carbon nanomaterials: production , impact on plant development , agricultural and environmental applications," Chem. Biol. Technol. Agric., pp. 1–26, 2016.
- [17] Kroto H. W, Heath J. R, O'Brien S. C, Curl R. F, and Smalley RE. C, "C60 - the thrid man," Nature, vol. 318, pp. 162–163, 1993.
- [18] T. Shoala, "Carbon nanostructures: Detection, controlling plant diseases and mycotoxins," Elsevier Inc., 2019.
- [19] Ahmad Aqel, Kholoud M. M. Abou El-nour, Reda A. A. Ammar, and Abdulrahman Al-warthan, "Carbon nanotubes, science and technology part (1) structure,synthesis and characterisation," Arab. J. Chem., vol. 5, no. 1, pp. 1–23, 2012.
- [20] S. Aman et al., "Magnetic field effect on poiseuille flow and heat transfer of carbon nanotubes along a vertical channel filled with casson fluid magnetic field effect on poiseuille flow and heat transfer of carbon nanotubes along a vertical channel filled with casson flu," vol. 7, 2017.
- [21] S. Kumar, R. Rani, N. Dilbaghi, and K. Tankeshwar, "Carbon nanotubes : a novel material for multifaceted applications in human healthcare," Chem. Soc. Rev., vol. 46, pp. 158–196, 2017.
- [22] P. Pandey and M. Dahiya, "Carbon nanotubes : types , methods of preparation and applications ," no. June, International journal of Phar. Scie. and Rese. , vol. 1, pp.15-21, 2016.
- [23] T. S. Gspann et al., "High thermal conductivities of carbon nanotube films and micro-fibres and their dependence on morphology," Carbon N. Y., vol. 114, no. 0, pp. 160–168, 2017.
- [24] P. Ajayan, R. Vajtai, "Properties and applications of carbon nanotubes.", pp.315-330, 2001.
- [25] T. H. E. Royal, S. Academy, and O. F. Sciences, "Compiled by the class for physics of the royal swedish academy of sciences graphene," vol. 50005, no. October, pp. 0–10, 2010.
- [26] A. Mondal and N. R. Jana, "Graphene-nanoparticle composites and their applications in energy , environmental and biomedical science," vol. 3, no. 3, pp. 177–192, 2014.

- [27] S. N. Alam, N. Sharma, and L. Kumar, "Synthesis of graphene oxide (GO) by modified Hummers method and its thermal reduction to obtain reduced graphene oxide (rGO)," *Graphene*, vol. 06, no. 01, pp. 1–18, 2017.
- [28] D. R. Dreyer, S. Park, W. Bielawski, and R. S. Ruoff, "The chemistry of graphene oxide," *Chemical society reviews*, vol.39, pp.228-240, 2010.
- [29] A. G. Kolhatkar, A. C. Jamison, D. Litvinov, and R. C. Willson, "Tuning the magnetic properties of nanoparticles," pp. 15977–16009, 2013.
- [30] M. Veith, "Material sciences," *Comptes Rendus Chim.*, vol. 7, no. 5, p. 431, 2004.
- [31] T. B. Leeuwen, "Chapter 3. diamagnetism," pp. 19–29, 2018.
- [32] M. Dresselhaus, "Solid state physics part iii magnetic properties of solids." pp.1-143, 2011.
- [33] S. P. Gubin, Y. A. Koksharov, G. B. Khomutov, and G. Y. Yurkov, "Magnetic nanoparticles : preparation , structure and properties," no. May 2014, vol.74, pp.539-574, 2005.
- [34] R. M. Cornell and U. Schwertmann, " The iron oxides: structure, properties, reactions, occurrences and uses, " *Nature*, vol.236, pp.285-286, 2003.
- [35] A. S. Teja and P. Koh, "Synthesis , properties , and applications of magnetic iron oxide nanoparticles," *Prog. Cryst. Growth Charact. Mater.*, vol. 55, no. 1–2, pp. 22–45, 2009.
- [36] S. Klotz, T. Strässle, J. Philippe, T. Hansen, and M. J. Wenzel, "Magnetism and the verwey transition in  $\text{Fe}_3\text{O}_4$  under pressure," pp. 2–5, 2008.
- [37] A. Fadli and A. Adnan, "Synthesis of magnetite nanoparticles via co-precipitation method," vol.622, 2019.
- [38] A. J. Antone and Z. Sun, "Preparation and application of iron oxide nanoclusters," pp. 1–16, vol.5, 2019.
- [39] M. QF , R.L, Z. Manuscript, "Macrophage membrane-coated iron oxide nanoparticles for enhanced photothermal tumor therapy," vol.29, pp.1-30, 2018.
- [40] A. Kostopoulou, I. Tsiaoussis, and A. Lappas, "Magnetic iron oxide nanoclusters with tunable optical response," vol. 9, pp. 201–206, 2011.
- [41] R. Nagarajan, M. Sciences, E. Team, and K. Street, "Nanoparticles : building blocks for nanotechnology," pp. 2–14, 2008.

- [42] Y. Zhang, N. Kohler, and M. Zhang, "Surface modification of superparamagnetic magnetite nanoparticles and their intracellular uptake," *Biomaterials*, vol. 23, no. 7, pp. 1553–1561, 2002.
- [43] O. E. Plastiras, E. Deliyanni, and V. Samanidou, "Applications of graphene-based nanomaterials in environmental analysis," *Appl. Sci.*, vol. 11, no. 7, 2021.
- [44] E. Tang, G. Cheng, X. Ma, X. Pang, and Q. Zhao, "Surface modification of zinc oxide nanoparticle by PMAA and its dispersion in aqueous system," *Appl. Surf. Sci.*, vol. 252, no. 14, pp. 5227–5232, 2006.
- [45] S. Islam, M. A. R. Bhuiyan, and M. N. Islam, "Chitin and chitosan: structure, properties and applications in biomedical engineering," *J. Polym. Environ.*, vol. 25, no. 3, pp. 854–866, 2017.
- [46] G. Moku, V. R. Gopalsamuthiram, T. R. Hoye, and J. Panyam, "Surface modification of nanoparticles: methods and applications," *Surf. Modif. Polym. Methods Appl.*, pp. 317–346, 2019.
- [47] E. Santiago de Alvarenga, "Characterization and properties of chitosan," *Biotechnol. Biopolym.*, no. June 2011, 2011.
- [48] J. Jhaveri, Z. Raichura, T. Khan, and M. Momin, "Chitosan nanoparticles-insight into properties, functionalization and applications in drug delivery and theranostics," pp. 1–29, 2021.
- [49] B. W. Kaplan and D. Ph, "Priority medicines for Europe and the world " A public health approach to innovation " Update on 2004 Background Paper Written by Warren Kaplan Background Paper 6 . 5 Cancer and Cancer Therapeutics," no. April, pp. 1–62, 2013.
- [50] A. P. Nikalje, "Nanotechnology and its applications in medicine," vol. 5, pp. 81–89, 2015.
- [51] H. Maeda, "Macromolecular therapeutics in cancer treatment: The EPR effect and beyond," *J. Control. Release*, pp. 1–7, 2012.
- [52] D. Pissuwan, S. M. Valenzuela, and M. B. Cortie, "Therapeutic possibilities of plasmonically heated gold nanoparticles," *Trends Biotechnol.*, vol. 24, no. 2, pp. 62–67, 2006.
- [53] J. D. Byrne, T. Betancourt, and L. Brannon-peppas, "Active targeting schemes for nanoparticle systems in cancer therapeutics," *Adv. Drug Deliv. Rev.*, vol. 60, no. 15, pp. 1615–1626, 2008.
- [54] S. Nie, "Understanding and overcoming major barriers in cancer nanomedicine opsonization & phagocytosis," vol. 5, no. 4, pp. 523–528, 2010.

- [55] D. Sleep, J. Cameron, and L. R. Evans, "Albumin as a versatile platform for drug half-life extension," *Biochim. Biophys. Acta - Gen. Subj.*, vol. 1830, no. 12, pp. 5526–5534, 2013.
- [56] A. Mahapatro and D. K. Singh, "Biodegradable nanoparticles are excellent vehicle for site directed in-vivo delivery of drugs and vaccines.," *J. Nanobiotechnology*, vol. 9, p. 55, 2011.
- [57] H. Ragelle, F. Danhier, V. Pr eat, R. Langer, and D. G. Anderson, "Nanoparticle-based drug delivery systems: a commercial and regulatory outlook as the field matures," *Expert Opin. Drug Deliv.*, vol. 14, no. 7, pp. 851–864, 2017.
- [58] S. Carregal-Romero, P. Guardia, X. Yu et al , "Magnetically triggered release of molecular cargo from iron oxide nanoparticle loaded microcapsules," *J. Nanoscale*, vol.7, pp. 570-576, 2015.
- [59] M. Khani et al., "RSC advances as an effective and non-corrosive oxidizing agent," *RSC Adv.*, vol. 6, pp. 115055–115057, 2016.
- [60] R. R. Amirov, J. Shayimova, Z. Nasirova, and A. M. Dimiev, "Chemistry of graphene oxide . reactions with transition metal cations," *Carbon N. Y.*, vol. 116, pp. 356–365, 2017.
- [61] S. Pei, Q. Wei, K. Huang, H. Cheng, and W. Ren, "Green synthesis of graphene oxide by seconds timescale water electrolytic oxidation," *Nat. Commun.*, pp. 1–9, 2018.
- [62] H. Rashid, M. A. Mansoor, B. Haider, R. Nasir, S. B. Abd Hamid, and A. Abdulrahman, "Synthesis and characterization of magnetite nanoparticles with high selectivity using in-situ precipitation method," *Sep. Sci. Technol.*, vol. 55, no. 6, pp. 1207–1215, 2020.
- [63] M. C. Mascolo, Y. Pei, and T. A. Ring, "Room temperature co-precipitation synthesis of magnetite nanoparticles in a large pH window with different bases," *Materials (Basel).*, vol. 6, no. 12, pp. 5549–5567, 2013.
- [64] T. Ahn, J. H. Kim, H. Yang, J. W. Lee, and J. Kim, "Formation pathways of magnetite nanoparticles by co-precipitation method," *physiacl Chem.*, no. 10, vol. 116, pp. 6069-6076, 2012.
- [65] M. Filippousi, M. Angelakeris, M. Katsikini et al., "Surfactant effects on the structural and magnetic properties of iron oxide nanoparticles," *J. phy. che.* , no. 29, vol. 118, pp. 16209-16217, 2014.
- [66] X. Yang, Y. Shang, Y.Li et al., "Synthesis of monodisperse iron oxide nanoparticles without surfactants," 2014.
- [67] S. Zhu et al., "Ultrasonics sonochemistry sonochemical fabrication of Fe<sub>3</sub> O<sub>4</sub> nanoparticles

- on reduced graphene oxide for biosensors,” *Ultrason. - Sonochemistry*, vol. 20, no. 3, pp. 872–880, 2013.
- [68] L. Shen, B. Li, and Y. Qiao, “Fe<sub>3</sub>O<sub>4</sub> nanoparticles in targeted drug/gene delivery systems,” *Materials (Basel)*, vol. 11, no. 2, pp. 1–29, 2018.
- [69] H. Metal and I. Removal, “Magnetic chitosan nanocomposites: a useful recyclable tool for heavy metal ion removal,” vol. 2, no. 5, pp. 3–8, 2009.
- [70] L. Liu et al., “Talanta preparation and characterization of chitosan / graphene oxide composites for the adsorption of Au ( III ) and Pd ( II ),” *Talanta*, vol. 93, pp. 350–357, 2012.
- [71] N. Ye, Y. Xie, P. Shi, T. Gao, and J. Ma, “Synthesis of magnetite / graphene oxide / chitosan composite and its application for protein adsorption,” *Mater. Sci. Eng. C*, vol. 45, pp. 8–14, 2014.
- [72] L. T. Tran, H. V Tran, T. D. Le, G. L. Bach, and L. D. Tran, “Studying Ni ( II ) Adsorption of Magnetite / Graphene Oxide / Chitosan Nanocomposite,” p p. 9, 2019.
- [73] H. V Tran, L. T. Bui, T. T. Dinh, D. H. Le, C. D. Huynh, and A. X. Trinh, “Graphene oxide / Fe<sub>3</sub>O<sub>4</sub> / chitosan nanocomposite: a recoverable and recyclable adsorbent for organic dyes removal . Application to methylene blue,” no. 3, vol. 4, 2017.
- [74] B. Zhang, R. Hu, D. Sun, T. Wu, and Y. Li, “Fabrication of chitosan / magnetite-graphene oxide composites as a novel bioadsorbent for adsorption and detoxification of Cr ( VI ) from aqueous solution,” no. June, pp. 1–12, 2018.
- [75] S. Kazemi, M. Pourmadadi, F. Yazdian, and A. Ghadami, “International journal of biological macromolecules the synthesis and characterization of targeted delivery curcumin using chitosan-magnetite-reduced graphene oxide as nano-carrier,” *Int. J. Biol. Macromol.*, vol. 186, no. June, pp. 554–562, 2021.
- [76] M. Atawneh, S. Makharza, S. Zahran, K. Titi, F. Takrori, and S. Hampel, “The cross-talk between lateral sheet dimensions of pristine graphene oxide nanoparticles and Ni<sup>2+</sup>adsorption,” *RSC Adv.*, vol. 11, no. 19, pp. 11388–11397, 2021.
- [77] X. Wang and W. Dou, “Preparation of graphite oxide (GO) and the thermal stability of silicone rubber/GO nanocomposites,” *Thermochim. Acta*, vol. 529, pp. 25–28, 2012.
- [78] L. M. Tung et al., “ Synthesis, characterizations of superparamagnetic Fe<sub>3</sub> O<sub>4</sub> –Ag hybrid nanoparticles and their application for highly effective bacteria inactivation ,” *J. Nanosci. Nanotechnol.*, vol. 16, no. 6, pp. 5902–5912, 2016.
- [79] Ö. Metin, Ş. Aydoğan, and K. Meral, “A new route for the synthesis of graphene oxide-

- Fe<sub>3</sub>O<sub>4</sub> (GO-Fe<sub>3</sub>O<sub>4</sub>) nanocomposites and their schottky diode applications,” *J. Alloys Compd.*, vol. 585, pp. 681–688, 2014.
- [80] R. Bissessur, P. K. Y. Liu, and S. F. Scully, “Intercalation of polypyrrole into graphite oxide,” *Synth. Met.*, vol. 156, no. 16–17, pp. 1023–1027, 2006.
- [81] P. Roonasi and A. Holmgren, “A study on the mechanism of magnetite formation,” pp. 829–836, 2009.
- [82] N. A. Hussien, N. Işıklan, and M. Türk, “Aptamer-functionalized magnetic graphene oxide nanocarrier for targeted drug delivery of paclitaxel,” *Mater. Chem. Phys.*, vol. 211, pp. 479–488, 2018.
- [83] N. K. Rukman, M. Jannatin, G. Supriyanto, M. Z. Fahmi, and W. A. W. Ibrahim, “GO-Fe<sub>3</sub>O<sub>4</sub> Nanocomposite from coconut shell: Synthesis and characterization,” *IOP Conf. Ser. Earth Environ. Sci.*, vol. 217, no. 1, 2019.
- [84] M. F. Queiroz, K. R. T. Melo, D. A. Sabry, G. L. Sasaki, and H. A. O. Rocha, “Does the use of chitosan contribute to oxalate kidney stone formation?,” *Mar. Drugs*, vol. 13, no. 1, pp. 141–158, 2015.
- [85] J. Kumirska et al., “Application of spectroscopic methods for structural analysis of chitin and chitosan,” *Mar. Drugs*, vol. 8, no. 5, pp. 1567–1636, 2010.
- [86] J. Zia and J. Pandey, “Preparation and characterization of iron- metal nanocomposite of chitosan: towards heterogeneous biocatalysts for organic reactions,” vol. 5, no. 2, pp. 101–105, 2018.
- [87] S. Kumar and J. Koh, “Physiochemical and optical properties of chitosan based graphene oxide bionanocomposite,” *Int. J. Biol. Macromol.*, vol. 70, pp. 559–564, 2014.
- [88] M. Aliabadi, H. Shagholani, and A. Yunessnia, “Synthesis of a novel biocompatible nanocomposite of graphene oxide and magnetic nanoparticles for drug delivery,” *Int. J. Biol. Macromol.*, 2017.
- [89] K. Mohanraj, G. Sivakumar, “Nanoparticles by sonochemical method,” vol. 46, no. 10, pp. 1935–1942, 2017.
- [90] F. He, J. Fan, D. Ma, L. Zhang, C. Leung, and H. L. Chan, “The attachment of Fe<sub>3</sub>O<sub>4</sub> nanoparticles to graphene oxide by covalent bonding,” *Carbon N. Y.*, vol. 48, no. 11, pp. 3139–3144, 2010.
- [91] M. Z. Kassae, E. Motamedi, and M. Majdi, “Magnetic Fe<sub>3</sub>O<sub>4</sub>-graphene oxide/polystyrene: fabrication and characterization of a promising nanocomposite,” *Chem. Eng. J.*, vol. 172, no. 1, pp. 540–549, 2011.

- [92] F. Emadi, A. Amini, A. Gholami et al., “Functionalized graphene oxide with chitosan for protein nanocarriers to protect against enzymatic cleavage and retain collagenase activity,” Nature Publishing Group, 2017.
- [93] M. Sneha and N. M. Sundaram, “Preparation and characterization of an iron oxide-hydroxyapatite nanocomposite for potential bone cancer therapy,” *Int. J. Nanomedicine*, vol. 10, pp. 99–106, 2015.
- [94] Y. Yao, S. Miao, S. Liu, L. P. Ma, H. Sun, and S. Wang, “Synthesis, characterization, and adsorption properties of magnetic Fe<sub>3</sub>O<sub>4</sub>/graphene nanocomposite,” *Chem. Eng. J.*, vol. 184, pp. 326–332, 2012.

## المُلخَص

في هذه الأطروحة قمنا بإعداد وتمييز حجمين من أكسيد الجرافيت النانوية (200 نانومتر و 450 نانومتر). بالإضافة إلى ذلك تم تحضير جزيئات أكسيد الحديد ذات الأساس المغناطيسي وتحميلها على أكسيد الجرافيت GO, وإضافة جزيئات الشيتوزان إلى أكسيد الجرافيت .

تم استخدام عملية الأكسدة والاختزال لصنع أكسيد الجرافيت (طريقة Hummers)، وتم تحديد المنتج النهائي كأكسيد الجرافيت (GO- 450 nm) و في ظل ظروف خاصة تم استخدام جهاز tip sonicator لتقليل حجم الجسيمات إلى 200 نانومتر, و بتفاعل كيميائي بسيط (co-precipitation) بين ( $Fe^{+3}$ ) و ( $Fe^{+2}$ ) أنتجت جزيئات أكسيد الحديد المغناطيسية تسمى  $Fe_3O_4$ .

يكشف التحليل الطيفي FT-IR ارتباط مجموعات الأكسجين المختلفة على سطح جسيمات الجرافيت ( أكسيد جرافيت 200 نانومتر و أكسيد جرافيت 450 نانومتر)، ويظهر طيف FT-IR الخاص بـ  $Fe_3O_4$  المحضر ذروة قوية عند حوالي 588 سم<sup>-1</sup> كدليل على تكون هذه الجزيئات المغناطيسية. كما و تظهر أطياف FT-IR لنظام (GO-200 nm/Cs/ $Fe_3O_4$ ) ذروة أكثر حدة من أطياف نظام (GO-450 nm/Cs/ $Fe_3O_4$ ). و كشف التحليل الطيفي المرئي للأشعة فوق البنفسجية للنظامين عن زيادة عرض النطاق الترددي مع تقليل حجم الجسيمات النانوية.